Petroleum Science 23 (2026) 7017–7036

Contents lists available at ScienceDirect

Petroleum Science

journal homepage: www.keaipublishing.com/en/journals/petroleum-science

Original Paper

Diagenesis and volcaniclastic influence on tight sandstone reservoir quality: Insights from the Shahezi Formation, Lishu Fault Depression, Songliao Basin, NE China

Shu-Yang Wang [a,b,c], Xuan-Long Shan [a,b,c], Chao-Fan Zhu [d], Wen-Tong He [a,b,c,*], Yi-Bo Wang [a,b,c], Ying Bian [a,b,c], Yu-Feng Shen [a,b,c], Nan Jiang [a,b,c], Xin-Tao Ma [a,b,c], Ze-Yu Ji [a], Qi-Xian Xie [e], De-Kun Zhu [e]

[a] College of Earth Sciences, Jilin University, Changchun, 130021, Jilin, China
[b] National Key Laboratory of Deep Earth Exploration and Imaging, Changchun, 130021, Jilin, China
[c] International Center of Future Science (ICFS), Jilin University, Changchun, 130012, Jilin, China
[d] College of Construction Engineering, Jilin University, Changchun, 130021, Jilin, China
[e] Zhejiang Geological and Mineral Exploration Institute Co., Ltd., Hangzhou, 310012, Zhejiang, China

ARTICLE INFO

Article history:
Received 8 September 2025
Received in revised form
2 November 2025
Accepted 6 September 2026
Available online 10 September 2026

Edited by Xiu-Fang Hu

Keywords:
Lishu Fault Depression
Shahezi Formation
Diagenetic facies
Volcaniclastic influence
Pore-structure evolution
Clay mineral transformation

ABSTRACT

Continental rift basins host prolific hydrocarbon resources; however, their tight sandstone reservoirs often undergo complex diagenetic modifications, resulting in significant heterogeneity and uncertainty in reservoir predictions. While the processes of compaction, cementation, and dissolution have been extensively documented, the influence of volcaniclastic input on diagenetic pathways and pore-system evolution remains inadequately constrained, which limits our understanding of reservoir quality in volcanic-influenced settings. In this study, we integrated core observations, blue-epoxy–impregnated thin sections, cathodoluminescence (CL), SEM–EDS, XRD, NMR, and micro-CT analyses to investigate the Shahezi Formation sandstones from on the northern slope of the Lishu Fault Depression in the Songliao Basin. We identified five diagenetic facies types: (1) tightly cemented (DFT-I), (2) moderately compacted with carbonate-cement dissolution (DFT-II), (3) moderately compacted with unstable-grain dissolution (DFT-III), (4) strongly compacted and densely cemented (DFT-IV), and (5) strongly compacted with intergranular dissolution (DFT-V). Quantitative pore-network characterization reveals that the dissolution of volcaniclastic grains and associated cements significantly enhanced porosity and connectivity in DFT-II and DFT-V, whereas DFT-I and DFT-IV experienced intense compaction and cementation, resulting in ultra-tight intervals. Illite-dominated clay assemblages found at burial depths greater than 4000 m and temperatures exceeding 160 °C indicate a late, high-temperature diagenetic stage. These findings demonstrate that volcaniclastic input plays a critical role in diagenetic evolution and reservoir heterogeneity in tight rift-basin sandstones. By incorporating the effects of volcaniclastic materials into diagenetic facies classification, we can improve reservoir quality predictions for the Shahezi Formation and establish a transferable framework applicable to tight sandstone systems across continental rift basins globally.

© 2026 The Authors. Publishing services by Elsevier B.V. on behalf of KeAi Communications Co. Ltd. This is an open access article under the CC BY license (http://creativecommons.org/licenses/by/4.0/).

1. Introduction

Continental rift basins are globally significant hydrocarbon provinces due to their abundant oil and gas resources (Bosworth, 1985). Their formation and evolution are strongly governed by tectonic activity, which produces complex depositional systems and rapid sedimentation. Such dynamic sediment supply

* Corresponding author
E-mail address: hewentong0510@163.com (W.-T. He).

Peer review under the responsibility of China University of Petroleum (Beijing).

https://doi.org/10.1016/j.petsci.2026.09.008

1995-8226/© 2026 The Authors. Publishing services by Elsevier B.V. on behalf of KeAi Communications Co. Ltd. This is an open access article under the CC BY license (http://creativecommons.org/licenses/by/4.0/).

introduces multiple provenance sources and depositional environments, resulting in pronounced sandstone heterogeneity and substantial challenges for reservoir characterization (Prosser, 1993; Gupta et al., 1998; Baudon et al., 2009). Tight clastic reservoirs in these basins generally exhibit poor petrophysical properties, intricate pore–throat architectures, and intense diagenetic modification driven by compaction, cementation, and dissolution (Xi et al., 2015; Lai et al., 2018; Al-Juboury et al., 2021; Wu et al., 2021). Although diagenesis has been widely recognized as a key factor controlling reservoir quality in deltaic systems, relatively limited attention has been paid to the combined influence of mixed sediment input and diagenesis on reservoir heterogeneity in fault-bounded rift settings (Lai et al., 2017). Consequently, the coupled effects of depositional conditions and diagenetic evolution on reservoir quality remain insufficiently understood, constraining accurate reservoir prediction across stratigraphic intervals in rift basins.

Recent advancements in reservoir characterization, analytical techniques, and experimental approaches have significantly enhanced the reconstruction of diagenetic processes. As a result, diagenesis has emerged as a central focus in tight sandstone studies, with diagenetic facies frameworks greatly improving our understanding of reservoir evolution (Hong et al., 2020; Santosh and Feng, 2020; Jabir et al., 2021; Zhao et al., 2021). Diagenetic evolution is typically categorized into early, mesogenetic, and late stages (Morad et al., 2010; Xi et al., 2019), each influenced by factors such as burial depth, fluid composition, and depositional environment (Hasnan et al., 2020; Su et al., 2022).

The Songliao Basin in northeast China is one of the largest and most prolific hydrocarbon-bearing rift basins in East Asia, serving as an ideal natural laboratory for tight sandstone research (Hou et al., 2011; Wang et al., 2025). The northern slope of the Lishu Fault Depression features delta-front sandstones of the Shahezi Formation, where reservoir evolution is influenced by both sediment supply and diagenesis. Recent studies have highlighted the significance of volcaniclastic input in altering diagenetic pathways and the evolution of pore systems in rift basins. Volcanic glass and unstable lithic fragments readily release labile cations (e.g., Fe^{2+}, Mg^{2+}, Ca^{2+}), which accelerate the transformation from smectite to illite and promote early carbonate and clay cementation, thereby reducing pore connectivity (Worden and Burley, 2003; Ding et al., 2020). Conversely, acidic diagenetic fluids can dissolve feldspar and volcanic components, generating secondary pores that locally enhance reservoir quality (Weibel et al., 2023; Zhang et al., 2024). Therefore, volcaniclastic input exerts both destructive (cementation) and constructive (dissolution) effects, with the balance between these competing processes fundamentally controlling pore evolution and reservoir heterogeneity. However, the diagenetic response of volcaniclastic-rich lacustrine rift sandstones, particularly under conditions of deep burial and high temperatures, remains inadequately constrained. This knowledge gap hinders the accurate prediction of high-quality reservoirs in the Songliao Basin and similar fault-bounded rift basins globally.

To address this issue, we acquired integrated datasets comprising well logs, core samples, 3D seismic data, and laboratory analyses. We utilized blue-epoxy–impregnated thin sections, X-ray diffraction (XRD), cathodoluminescence (CL), scanning electron microscopy (SEM), nuclear magnetic resonance (NMR), and micro-computed tomography (micro-CT) to investigate lithologic features, pore evolution, diagenetic processes, and their impacts on reservoir quality. By establishing classifications of diagenetic facies, reconstructing diagenetic sequences, and quantifying pore-network evolution, this study elucidates the genetic mechanisms that control tight sandstone reservoirs and enhances the prediction of favorable reservoir intervals in volcaniclastic-rich rift settings.

2. Geological setting

The Songliao Basin is a large continental hydrocarbon-bearing basin located in northeastern China, characterized by a superimposed rift–sag structural framework. It ranks among the most prolific non-marine sedimentary basins globally in terms of oil and gas resources (Hu et al., 2005; Feng et al., 2011; Cao and He, 2020). The evolution of the basin can be categorized into three major stages: an early rifting phase, a subsequent post-rift thermal subsidence phase, and a later tectonic inversion phase. Vertically, it exhibits a typical rift–sag stratigraphic superposition, while laterally, six first-order tectonic units can be identified (Feng et al., 2015) (Fig. 1(a) and (b)).

The Lishu Fault Depression, situated in the Southeastern Uplift of the Songliao Basin, represents a fault-controlled, half-graben depression characterized by a west-bounding fault and eastward overlapping strata, which together form a composite spoon-shaped geometry (Chen, 1996) (Fig. 1(c) and (e)). It contains six third-order tectonic units, with the Sangshutai Fault serving as the principal boundary fault that governs sedimentation on the northern slope. Additionally, multiple NW- and SE-trending secondary faults have developed in the region (Wang et al., 2015, 2017) (Fig. 1(d)). During the early rifting stage, intense tectonism coincided with vigorous volcanism, leading to widespread deposition of the Huoshiling and Yingcheng volcanic units, as well as the accumulation of organic-rich lacustrine mudstones of the Shahezi Formation (Zhang et al., 2022).

The successions within the Lishu Fault Depression are relatively complete (Fig. 2). The Huoshiling Formation (J_1h) rests upon the basement and is characterized by a basal layer of volcanic rocks. It is subsequently overlain by the Shahezi Formation of mudstones interbedded with sandstones and conglomerates that was deposited during a period of intense tectonic activity and had a thickness exceeding 4000 m at the depocenter. The lithologies present include conglomerates, fine sandstones, silt-rich mudstones, and mudstones, accompanied by significant volcaniclastic input. Additionally, the Shahezi Formation contains high-quality organic-rich source rocks that exhibit strong hydrocarbon generation potential. Above this, the Yingcheng Formation is predominantly composed of clastic deposits, while the Denglouku Formation signifies a phase of reduced tectonic activity and is primarily made up of grayish-white fine sandstones interbedded with gray mudstones.

The basin-scale tectonic and thermal conditions established a fundamental diagenetic framework for reservoir evolution within the Shahezi Formation. Regionally, this formation underwent significant deep burial (4000 m) and experienced elevated burial temperatures (160 °C), indicative of advanced mesodiagenetic conditions. Intense volcanic activity contributed abundant volcaniclastics and heat, which accelerated the transformation of clay minerals (from smectite to illite) and promoted the generation of organic acids during the maturation of source rocks (Weibel et al., 2020). These acidic fluids facilitated the dissolution of feldspar and volcanic lithic fragments, resulting in the formation of localized secondary porosity. Concurrently, labile cations released from volcanic components (e.g., Fe^{2+}, Mg^{2+}, Ca^{2+}) altered pore-fluid chemistry and enhanced carbonate and illite cementation during mesodiagenesis (Gao et al., 2015). As a result, the northern slope of the Lishu Fault Depression exhibits distinct compaction–cementation features with localized dissolution enhancement, leading to highly heterogeneous diagenetic characteristics.

3. Sampling and methodology

3.1. Sampling

In the study area, a total of 23 exploration wells have been drilled, the majority of which contain natural gamma-ray, acoustic,

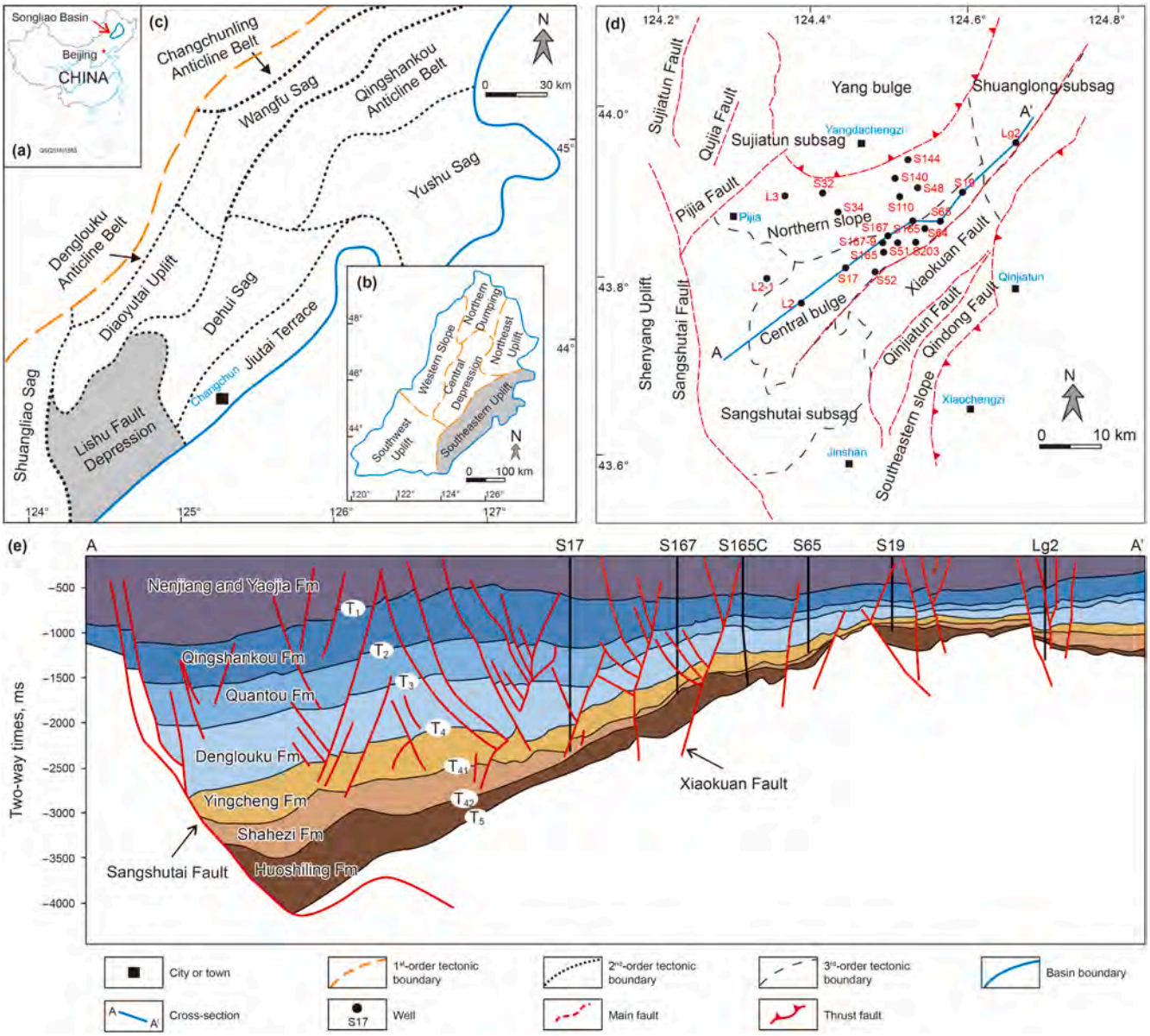


Fig. 1. Geological setting of the study area. **(a)** Location of the Songliao Basin in China; **(b)** first-order tectonic units of the Songliao Basin, focusing on the Southeastern Uplift; **(c)** location of the Lishu Fault Depression (a second-order tectonic unit, the study area) in the Southeastern Uplift; **(d)** fault system, third-order tectonic units, and well locations in the Lishu Fault Depression; **(e)** seismic interpretation of the profile A–A' across the northern slope. The stratigraphy includes the Upper Jurassic Huoshiling Formation (Fm), the Lower Cretaceous Shahezi, Yingcheng, and Denglouku formations, as well as the Upper Cretaceous Quantou, Qingshankou, and Yaojia formations. Modified from Wang et al. (2025).

resistivity, and density logs provided by the Sinopec Northeast Oil and Gas Branch. Continuous cores were recovered from Wells S17, S48, S203, S64, S110, and L3. These cores were analyzed for grain-size variation, sedimentary structures, and bedding characteristics. Representative core samples were selected for laboratory analyses, all of which are sandstones derived from fan-delta deposits within the Shahezi Formation.

3.2. Methodology

This study integrates various methodologies, including blue-epoxy–impregnated thin-section petrography, laser particle-size analysis, scanning electron microscopy (SEM), X-ray diffraction (XRD), carbonate carbon–oxygen isotope analysis, digital image analysis, nuclear magnetic resonance (NMR), micro-CT imaging, and routine core analysis (porosity and permeability), to systematically characterize reservoir properties.

(a) Blue-epoxy–impregnated thin-section petrography

Blue-epoxy–impregnated thin sections were employed to identify pore types, pore–throat distribution, and diagenetic textures. The pores were vacuum-impregnated with blue resin, and the thin sections (less than 0.03 mm) were stained with Alizarin Red to differentiate carbonate minerals. Observations were conducted using a Leica D05GS005 petrographic microscope (Arvidson and Mackenzie, 1999). A total of 60 thin sections were prepared from tight sandstone samples.

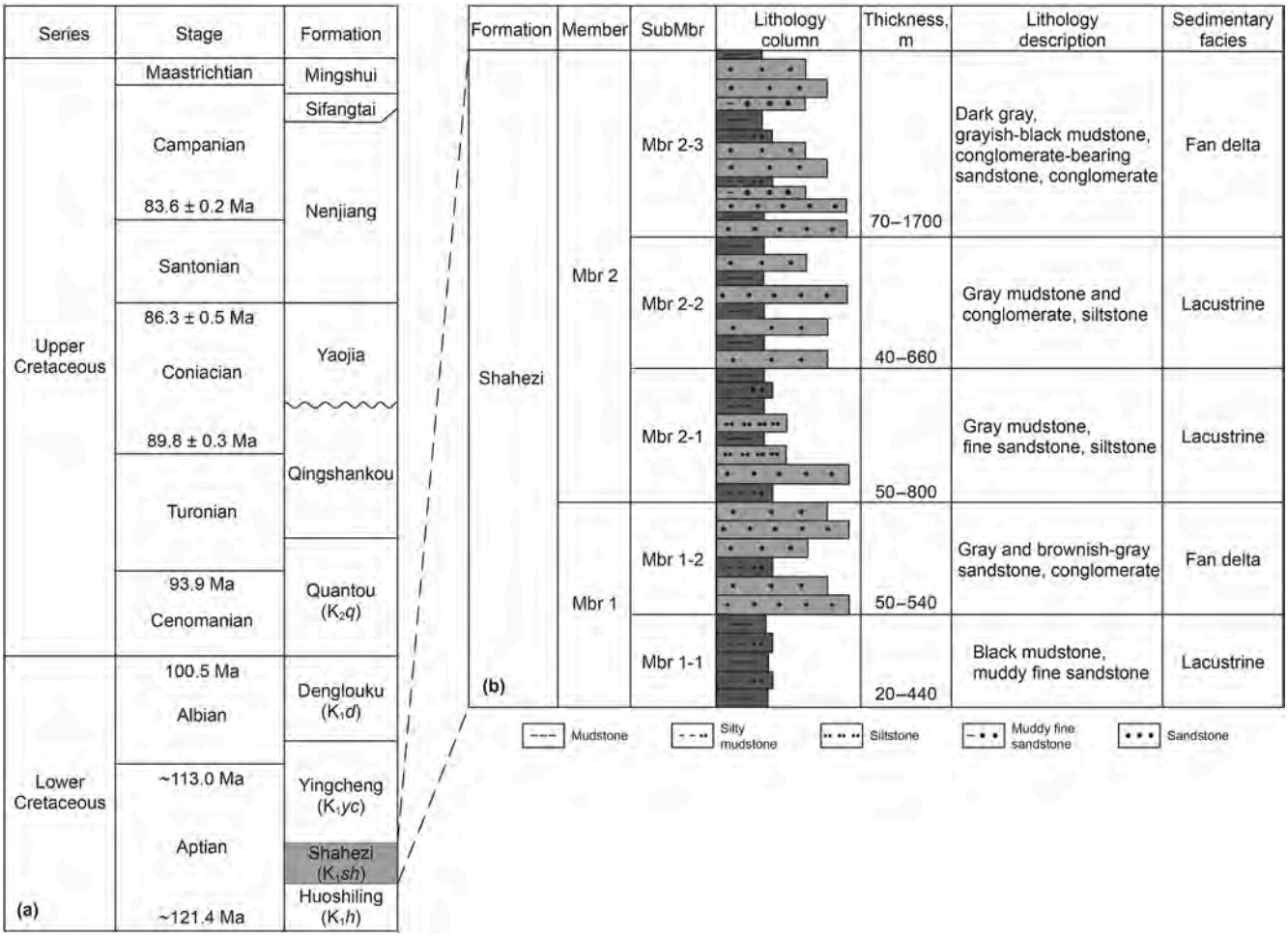


Fig. 2. (**a**) Chronostratigraphic chart showing the Upper Mesozoic in the Songliao Basin; **(b)** stratigraphic column showing the Lower Cretaceous Shahezi Formation on the northern slope of the Lishu Fault Depression. Grain-size scale: vf, very fine; f, fine; m, medium; c, coarse. Modified from Wang et al. (2025).

(b) Laser particle-size analysis

Grain-size distributions were measured using a Malvern Mastersizer 3000 laser diffraction analyzer (0.1–2500 μm), in accordance with ISO 13320:2020. A total of 56 core samples from five wells were analyzed to quantify grain-size parameters.

(c) SEM and energy-dispersive spectroscopy (EDS)

Microstructural and compositional features were examined using a ZEISS EVO 18 tungsten-filament SEM equipped with an Oxford X-MaxN 80 EDS system. Fourteen clay-rich sandstone samples from ten wells were selected to investigate authigenic mineral morphology, grain-contact relationships, and elemental compositions.

(d) Cathodoluminescence (CL) analysis

CL analysis was performed on polished thin sections from 16 tight sandstone samples to identify the types of carbonate cement and their growth zonation. Images were captured using an ELM-3R cathodoluminescence system coupled with a Leica DMLP microscope.

(e) Carbon and oxygen isotope analysis

Stable carbon and oxygen isotopes were analyzed using continuous-flow isotope ratio mass spectrometry (Spötl, 2011). Eighteen carbonate samples from two wells were evaluated with an Elementar Isoprime isotope ratio mass spectrometer. The powders were flushed with high-purity helium and reacted with phosphoric acid at 60 °C. Results were calibrated to the VPDB and LSVEC standards (Coplen et al., 2006) with a precision of ±0.05‰.

(f) Digital image analysis

Sixty samples were analyzed utilizing the CIAS-SU-ZL 3.0 color image system. Pore and throat characteristics were quantified through image segmentation to classify reservoir space types.

(g) Nuclear magnetic resonance (NMR)

NMR analyses were conducted using a MesoMR12-060H-I system in accordance with SY/T 6490-2023. Measurements were taken at 0.3 T and 1–42 MHz. T_2 relaxation spectra were inverted to derive pore-size distributions and connectivity (Song et al., 2022).

(h) Micro-computed tomography (micro-CT)

Three-dimensional (3D) pore structures were imaged using a ZEISS Xradia 520 Versa micro-CT at the State-Local Joint Engineering Laboratory for In-Situ Conversion and Drilling of Oil Shale, Jilin University. Cylindrical plugs (2.5 cm × 2.5 cm) were scanned, and volumes were reconstructed using XRM Reconstructor with

filtered back-projection, followed by processing in Avizo 9 for quantitative pore-network characterization (Schlüter et al., 2014; Zhang et al., 2016).

4. Results

4.1. Petrology and sedimentology

4.1.1. Sedimentary textures from core observations

Core observations reveal diverse sedimentary textures and bedding features along the northern slope (Fig. 3). The sandstones of the Shahezi Formation are predominantly composed of conglomerates, pebbly sandstones, lithic sandstones, siltstones, and medium sandstones. These are characterized by coarse grain size, poor sorting, and low rounding, which indicate low textural maturity. Massive bedding is prevalent, occasionally accompanied by horizontal lamination, cross-bedding, as well as both normal and reverse grading. In Well S110 (Fig. 3(d)), massive-bedded medium sandstones transition upward into parallel-bedded sandstones and tuffaceous siltstones. Pyrite enrichment is noted in fine sandstones from Well S203 (Fig. 3(e)). Well S17 exhibits second- and third-order erosional surfaces (Fig. 3(b)) and massive fine sandstones with black volcanic ash cement and reddish carbonate cement, containing clasts up to 3 cm (Fig. 3(a)). Collectively, these sedimentological characteristics indicate rapid deposition and frequent fluctuations in sediment supply, which are typical of fan-delta successions.

4.1.2. Grain-size characteristics

The Shahezi Formation was deposited within fan-delta systems characterized by fan-delta fronts and shore–shallow lake environments. Grain-size analysis reveals median grain size values ranging from 0.116 mm to 0.391 mm, with an average of 0.228 mm, which is consistent with gravelly fine sandstones. The mean sorting coefficient (S_o) derived from 56 samples across five wells is 1.886 (Table 1). Utilizing the sorting–porosity relationship, the original porosity was estimated to be 33.05%.

4.1.3. Compositions of tight sandstones

Quantitative modal petrography was employed to ascertain the framework composition, and sandstone classification adhered to the QFL and Lv–Lm–Ls ternary diagrams that are commonly utilized in volcaniclastic-rich systems (Folk et al., 1970; Pettijohn et al., 1987; Critelli et al., 2017). The results indicate that the sandstones of the Shahezi Formation are predominantly feldspathic litharenites (Fig. 4). The quartz content ranges from 33.80% to 73.50% by volume (mean 67.18%), feldspar from 12.30% to 27.60% by volume (mean 15.30%), and lithics from 11.20% to 41.18% by volume (mean 17.52%). Volcanic lithics are the dominant component of the lithic fraction, accompanied by polycrystalline quartz and minor sedimentary lithics, reflecting significant tectonic input and intensive volcaniclastic supply.

Table 1
Sorting coefficients and calculated original porosity of sandstone samples.

Well	No. of samples	Depth, m	S_o	Original porosity, %
S17	12	4175.99–4259.95	1.88	33.09
S64	12	2057.00–2109.00	1.74	34.07
S48	14	1576.50–1751.00	2.04	32.14
S110	8	1868.80–1967.00	2.10	30.86
S203	10	2155.00–2237.86	1.67	34.62

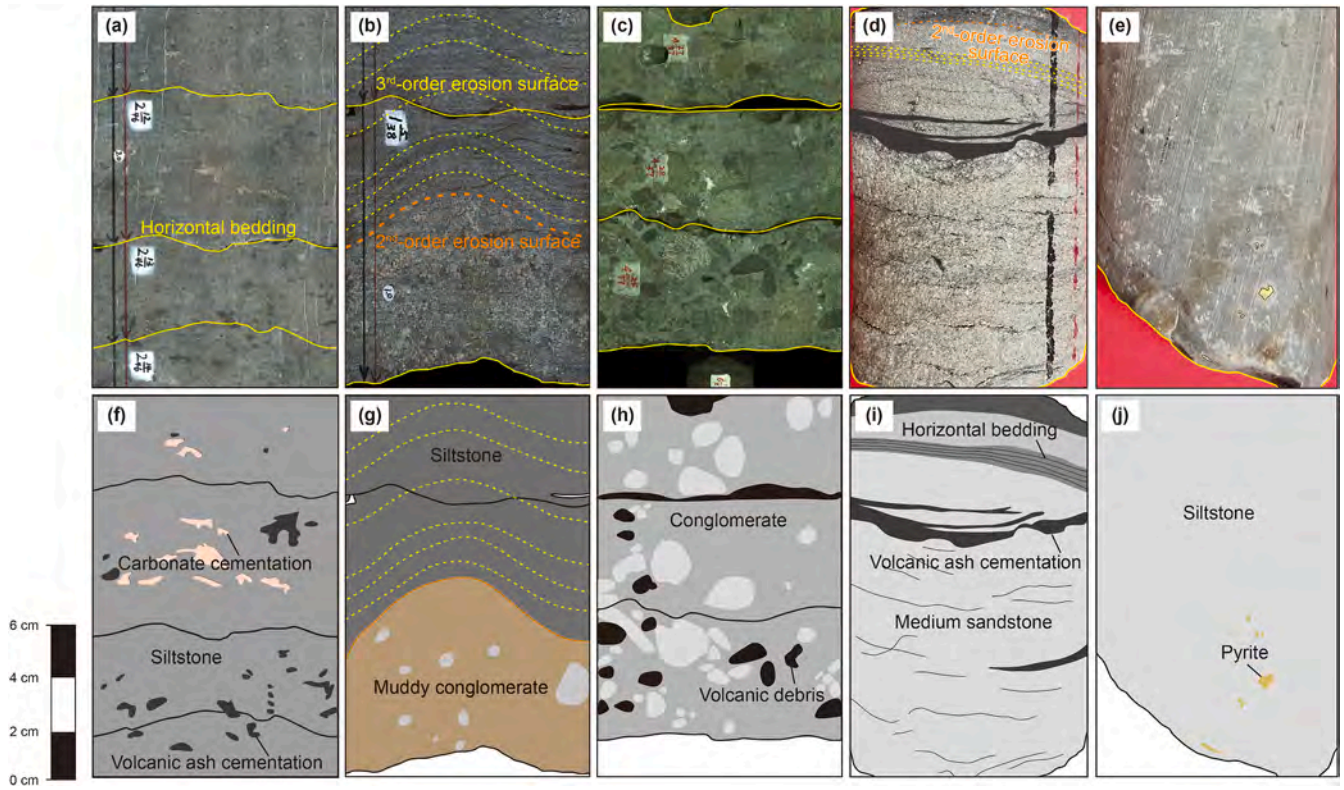


Fig. 3. Presents representative core photographs and sketches that illustrate massive gravely sandstones, graded bedding, matrix-supported conglomerates, and traction structures that are characteristic of fan-delta deposits.

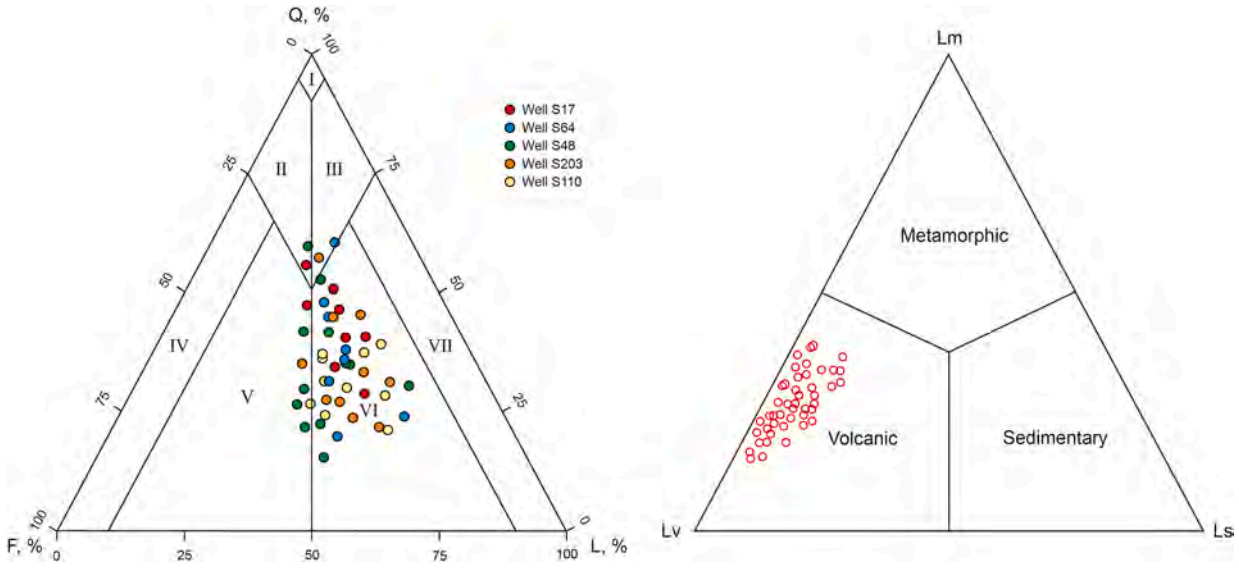


Fig. 4. QFL and Lv–Lm–Ls ternary plots indicating feldspathic litharenite composition with abundant volcanic lithics. Abbreviations: Q, quartz; F, feldspar; L, lithic fragments; Lm, metamorphic lithics; Lv, volcanic lithics; Ls, sedimentary lithics.

4.1.4. Pore types of tight sandstones

The sandstone reservoirs in the study area exhibit a variety of reservoir spaces, comprising both pores and fractures, which serve as storage capacity for hydrocarbons and pathways for fluid migration, thereby influencing the overall reservoir quality (Lai et al., 2016; Qiao et al., 2020; Wang et al., 2020). Consequently, understanding the primary pore types and their distribution is essential for comprehensive diagenetic characterization and the identification of 'sweet spots'. Based on the analysis of casting thin sections and scanning electron microscopy (SEM) observations, four distinct pore types were identified: primary intergranular pores (Fig. 5(a)), intergranular dissolution pores (Fig. 5(a)), intragranular dissolution pores (Fig. 5(b) and (d)), and microfractures (Fig. 5(b) and (e)). Primary intergranular pores, which are significant storage spaces formed between grains not completely occluded by diagenetic cements, constitute the predominant pore type in sandstones (Liu et al., 2020; Qiao et al., 2020). These pores typically exhibit irregular shapes and are located at grain contacts, with minimal dissolution residues. Secondary pores encompass both intergranular and intragranular dissolution pores. Intergranular dissolution pores consist of grain-edge dissolution pores and cement-dissolution pores, while intragranular dissolution pores are formed within feldspar and lithic fragments. Their irregular morphology reflects mineral–fluid reactions during diagenesis, with dissolution residues often remaining within the pores. Additionally, microfractures are present, including structural fractures induced by tectonic stress and dissolution fractures generated by diagenetic fluids.

4.1.5. Porosity and permeability characteristics

A total of 171 core plug analyses from Wells S17, S64, S48, S203, and S110 reveal porosity values ranging from 2.52% to 14.51%, with an average of 6.93%. The permeability values span from 0.002 mD to 10.841 mD, averaging at 0.638 mD. The porosity values predominantly cluster between 4% and 10%, while permeability primarily ranges from 0.01 mD to 0.5 mD (Fig. 6), thereby confirming the typical characteristics of tight sandstone.

4.2. Diagenesis analysis

Integrated petrographic observations, including blue-epoxy–impregnated thin sections, scanning electron microscopy (SEM), and cathodoluminescence (CL), demonstrate that the sandstones of the Shahezi Formation have undergone a combination of destructive processes, such as mechanical compaction and cementation, alongside constructive mechanisms, including dissolution and microfracturing. These diagenetic pathways collectively influence pore evolution and reservoir quality.

4.2.1. Compaction

Mechanical compaction progressively reduces primary porosity under increasing vertical and horizontal stress (Bai et al., 2018). As burial occurs, grain contacts evolve from point contacts to elongated and ultimately sutured contacts, accompanied by grain breakage and the plastic deformation of lithic fragments. In intervals that were cemented early by carbonates, compaction was locally inhibited, allowing for the preservation of point contacts, which reflects mechanical stabilization prior to deep burial. When the effective stress exceeds hydrostatic pressure, pressure-solution fringes develop at grain boundaries, releasing silica that precipitates as quartz overgrowths (Fig. 5(d) and (f)). Thus, compaction and pressure solution are the primary destructive diagenetic processes, significantly reducing pore volume and permeability.

4.2.2. Dissolution

Dissolution was primarily driven by organic acids generated during hydrocarbon maturation, alongside formation waters in deeply buried settings. This process resulted in the creation of secondary reservoir space, including intragranular and intergranular dissolution pores, as well as moldic pores, which substantially enhance pore connectivity and reservoir quality (Lai et al., 2016; Du et al., 2019; Qiao et al., 2020). The principal dissolved constituents include feldspars, volcanic lithics, and carbonate cements (Fig. 5(b)–(d)). The abundant presence of volcanic lithics and feldspar phenocrysts in the Shahezi sandstones renders them highly susceptible to acid-mediated dissolution, significantly

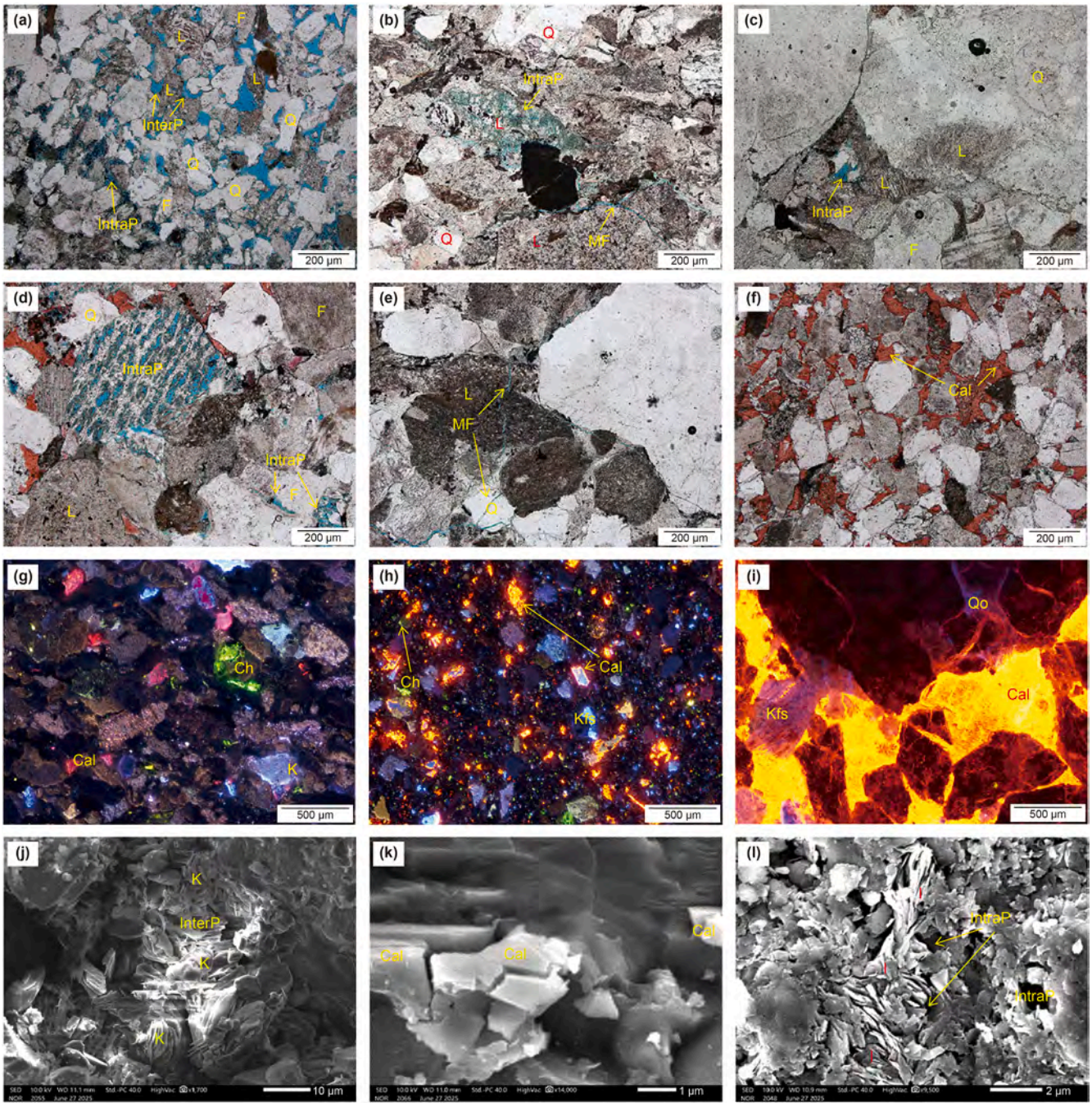


Fig. 5. Petrographic and microstructural characteristics of the Shahezi sandstones. **(a–c)** Intergranular and intragranular pores; **(d–f)** carbonate cement occluding pore systems; **(g–i)** CL images showing feldspar alteration and quartz overgrowths; **(j–l)** SEM images showing kaolinite, illite, and calcite pore fills. Abbreviations: Q, quartz; F, feldspar; L, lithics; Qo, quartz overgrowth; Cal, calcite; K, kaolinite; I, illite; Ch, chlorite; Kfs, K-feldspar; InterP, intergranular pore; IntraP, intragranular pore; MF, microfracture.

contributing to the development of secondary porosity and the formation of local reservoir sweet spots.

4.2.3. Cementation: carbonate, siliceous, and authigenic clay mineral cements

Cementation refers to the crystallization and precipitation of authigenic minerals, such as silica and carbonates, from pore fluids, which fill and enlarge pores, progressively binding loose sediments into rock. Cementation can occur throughout the diagenetic process; however, early cementation often results in further pore reduction and reservoir deterioration. Based on analyses of blue-epoxy–impregnated thin sections, SEM–EDS, cathodoluminescence (CL), and XRD, three major types of cementation were identified in the sandstones of the Shahezi Formation: carbonate cementation (Fig. 5(d), (f), (h), and (k)), authigenic clay mineral cementation (Fig. 5(g), (j), and (l)), and siliceous cementation (Fig. 5(c) and (i)). For instance, SEM–EDS analysis revealed calcite occluding intergranular pores between feldspar and quartz grains, with crystals exhibiting diverse morphologies (Fig. 5(k)).

Carbonate cementation is the most significant type affecting reservoir quality in the study area. It can be broadly divided into

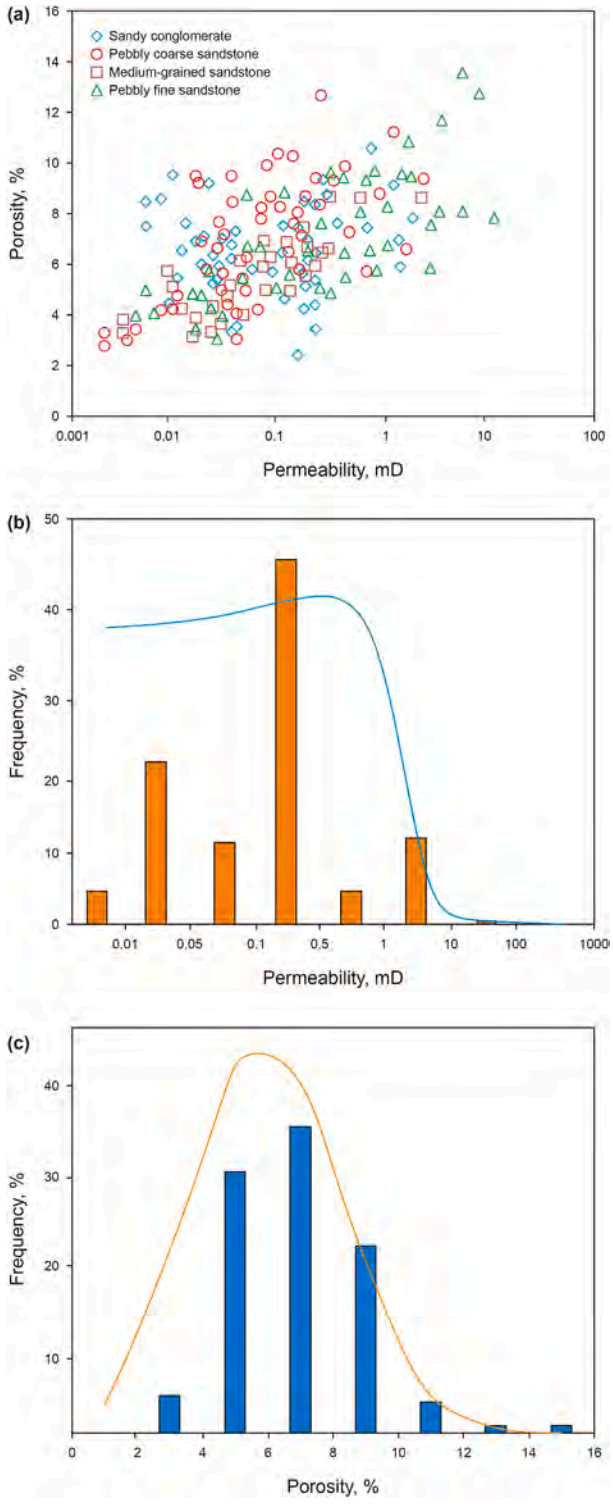


Fig. 6. Petrophysical characteristics of the Shahezi sandstones: **(a)** porosity–permeability cross-plot; **(b)** porosity histogram; **(c)** permeability histogram.

early and late phases according to diagenetic stages. Early carbonate cements, primarily calcite, precipitated during the early diagenetic stage B, characterized by weak compaction and grains typically displaying point contacts. In contrast, late carbonate cements, predominantly ferroan calcite, formed under strong compaction during the mesogenetic stage (from A2 to B), when

Table 2
Quantitative and petrographic criteria for diagenetic facies classification in the Shahezi Formation.

Facies	Porosity, %	Permeability, mD	Carbonate cement, vol.%	Silica cement index (0–3)	NMR movable fluid fraction, %	Median throat radius, μm	Coordination number	Dissolution index (0–3)	Compaction class	Dominant pore types	Reservoir quality
DFT-I	<3	<0.01	20	2–3	<5	<0.5	0.16	0–1	L–Su (linear–suture)	Cement-filled, minor intragranular	Very poor
DFT-II	4–12	0.05–0.5	5–15 (part dissolved)	1–2	6–12	1.0–2.0	1.42	2–3	P–L (point–linear)	Secondary pores, microfractures	Best
DFT-III	4–11	0.02–0.2	<10	1–2	8–15	0.8–1.5	1.87	2–3	P–L	Secondary intragranular	Good–fair
DFT-IV	<4	<0.01	10–25	2–3	<5	<0.5	0.20	0–1	L–Su	Compaction seams, residual infill	Very poor
DFT-V	4–8	0.01–0.08	3–12	1–2	5–10	0.6–1.2	1.18	1–2	L (linear)	Irregular secondary pores, clay films	Fair

Silica cement index (0–3): 0 = none; 1 = thin grain-rim overgrowths; 2 = continuous overgrowths; 3 = thick overgrowths/prominent secondary enlargement (distinct under CL).
Dissolution index (0–3): 0 = none; 1 = localized; 2 = widespread; 3 = strong/interconnected dissolution pores.
Compaction class: P = point contacts; L = long/linear contacts; Su = sutured contacts, reflecting increasing compaction intensity.

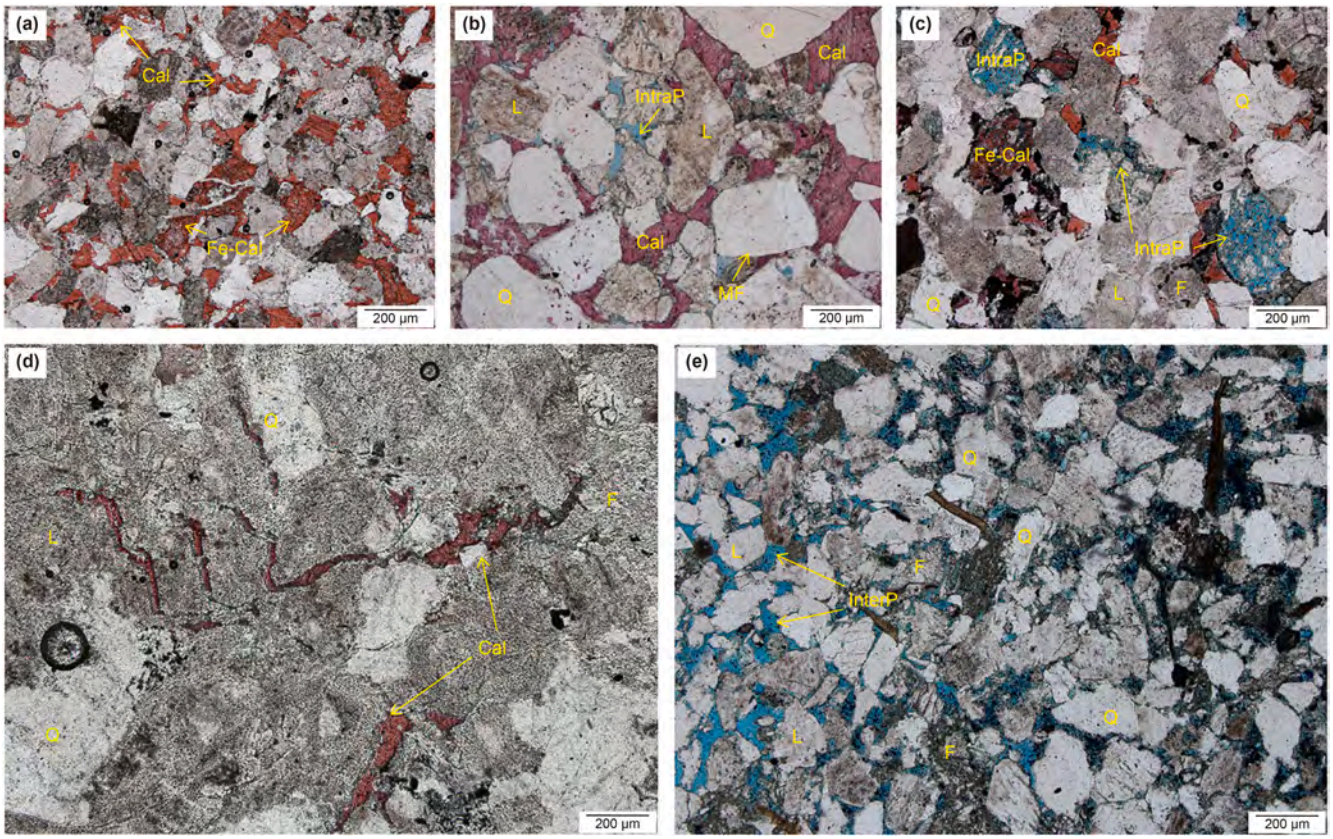


Fig. 7. Representative blue-epoxy–impregnated thin sections illustrating diagenetic facies of the Shahezi Formation, classified according to the quantitative criteria in Table 2. Facies include tightly cemented, carbonate-dissolution, unstable-grain-dissolution, densely compacted, and dissolution-enhanced types. Abbreviations: Q, quartz; F, feldspar; L, lithics; Fe-Cal, ferroan calcite; InterP, intergranular pore; IntraP, intragranular pore; MF, microfracture.

grains typically exhibited linear or concavo–convex contacts. To evaluate the effect of carbonate cementation on reservoir quality, 60 thin sections from seven wells were analyzed, revealing a total carbonate content ranging from 0 to 53 vol.% (mean 13.46 vol.%), with calcite and ferroan calcite as the dominant cement species.

Authigenic clay mineral cementation is predominantly characterized by kaolinite, illite, and minor montmorillonite, which commonly infill pores and microfractures. Scanning Electron Microscopy (SEM) reveals kaolinite as either booklets or vermicular aggregates (Fig. 5(j)), while illite is observed as irregular fine flakes (Fig. 5(l)). The crystallinity of illite increases with burial depth, tending toward sericitization, and it typically occupies intergranular and intragranular dissolution pores created by the alteration of feldspar and lithic fragments. Chlorite is relatively rare, likely due to a limited supply of Fe–Mg and the relatively acidic pore waters that disfavor chlorite formation while promoting kaolinite and illite.

Siliceous cementation is primarily manifested through quartz overgrowths. Blue-epoxy thin sections and cathodoluminescence (CL) images reveal pervasive overgrowth rims extending from grain boundaries, thus reducing pore volume (Fig. 5(c) and (i)). In addition to carbonate cementation, silica cementation (in the form of quartz overgrowths) and authigenic clay minerals significantly influence pore evolution. Furthermore, quartz dissolution followed by silica re-precipitation under acidic diagenetic conditions has been documented in tight sandstones (Liu et al., 2025), which is consistent with the localized dissolution features observed in this study.

Collectively, these observations indicate that carbonate, siliceous, and clay-mineral cementation—coupled with localized acidic dissolution—jointly control pore evolution and ultimately govern reservoir quality in the Shahezi Formation tight sandstones.

4.3. Diagenetic facies classification

To enhance the reproducibility and transparency of diagenetic facies classification, three quantitative indices were employed: the apparent compaction ratio (R_{com}), the apparent cementation ratio (R_{cem}), and the apparent dissolution ratio (R_{dis}), supported by

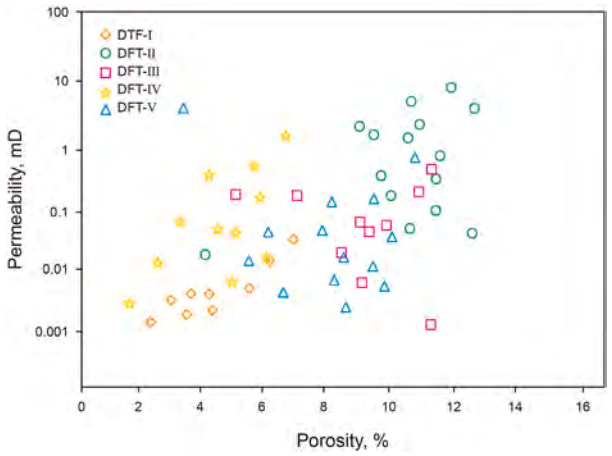


Fig. 8. Porosity–permeability cross-plot of the five diagenetic facies, showing strong heterogeneity controlled by compaction, dissolution, and cementation.

petrographic and micro-CT observations. The diagnostic thresholds and petrographic criteria used to distinguish the five diagenetic facies (DFT-I to DFT-V) are summarized in Table 2. These facies include tightly cemented facies (DFT-I), moderately compacted facies with dissolved carbonate cement (DFT-II), moderately compacted facies exhibiting unstable-grain dissolution (DFT-III), strongly compacted and densely cemented facies (DFT-IV), and strongly compacted facies characterized by intergranular dissolution (DFT-V) (Fig. 7). This classification scheme directly reflects the dominant genetic mechanisms and pore evolution pathways associated with each facies.

4.4. Pore structure characterization of different diagenetic facies types

To further evaluate reservoir-quality differences among diagenetic facies, quantitative pore-structure parameters were extracted through digital image analysis, nuclear magnetic resonance (NMR) tests, and 3D micro-computed tomography (micro-CT) reconstruction. These data provide multi-scale evidence linking pore architecture to diagenetic processes.

4.4.1. Petrophysical properties of different diagenetic facies

Porosity–permeability cross-plot distinctly reveals varying petrophysical behaviors among the five diagenetic facies (Fig. 8). DFT-I exhibits the poorest reservoir properties due to pervasive carbonate cementation, resulting in largely occluded pores and permeability typically less than 0.06 mD. In contrast, DFT-II and DFT-III develop secondary dissolution pores associated with the dissolution of feldspar grains and carbonate cement, leading to improved porosity and moderate permeability. DFT-IV is characterized by intense compaction and cementation, yielding low porosity (average 4.22%) and negligible permeability. Although DFT-V experienced similarly strong compaction, subsequent intergranular and lithic dissolution enhanced pore connectivity to some extent, resulting in a higher average porosity (6.12%) compared to DFT-IV.

4.4.2. Two-dimensional pore-structure characteristics

Digital image segmentation of 60 thin-section samples reveals significant contrasts in pore abundance, pore–throat size, and connectivity that are controlled by facies (Table 3; Fig. 9(a)–(e)). Facies DFT-I, represented by a casting thin section from Well S32 at a depth of 2701.64 m, shows pores that are almost completely occluded by ferroan calcite cement, resulting in a plane porosity of only 2.43%. In contrast, Facies DFT-II exhibits superior reservoir properties; a thin section from Well L3 at 3405 m reveals 1143 pores with a plane porosity of 5.64%. Facies DFT-III, represented by a sample from Well S52 at 3205 m, displays conditions similar to DFT-II, with secondary dissolution pores primarily formed by the dissolution of unstable grains (e.g., feldspar and calcite), and a plane porosity of 5.72%. Both Facies DFT-IV and DFT-V have undergone intense compaction, leading to a near-complete loss of primary porosity. However, due to variations in carbonate cementation and secondary dissolution, DFT-V demonstrates better petrophysical properties than DFT-IV. In DFT-IV, only 336 pores were identified, with pore radii ranging from 2.74 μm to 126.6 μm (average 43.49 μm). Overall, facies characterized by larger throat radii and more homogeneous pore structures exhibit superior reservoir quality. Specifically, facies with larger average throat radii and more uniform pore distributions, particularly DFT-II, exhibit the most favorable pore-network properties.

Table 3
Two-dimensional pore-structure parameters of different diagenetic facies derived from digital image analysis. DFT: diagenetic facies type; φ: porosity, %; K: permeability, mD; φ_p: plane porosity, %; N_p: total number of pores; Φ_{maxp}: maximum pore diameter, μm; Φ_{minp}: minimum pore diameter, μm; Φ_{averp}: average pore diameter, μm; N_t: total number of throats; Φ_{maxt}: maximum throat diameter, μm; Φ_{avert}: average throat diameter, μm; η: mean pore–throat ratio, dimensionless; N_C: average coordination number; C_m: average coefficient.

DFT	Lithology	φ, %	K, mD	φ_p, %	N_p	Φ_{maxp}, μm	Φ_{minp}, μm	Φ_{averp}, μm	N_t	Φ_{maxt}, μm	Φ_{avert}, μm	η	N_C	C_m
DFT-I	Pebbly fine sandstone	2.52–6.27 /3.58	0.008–0.03 /0.017	1.04–4.98 /3.36	566–945 /780	74.3–105.7 /92.4	3.62–9.29 /4.86	29.43–67.3 /33.65	42–65/48	28.3–37.5 /35.53	5.47–7.94/7.18	4.93–5.75 /5.53	0.12–0.36 /0.27	0.26–0.43 /0.37
DFT-II	Sandy conglomerate	4.25–12.6 /7.43	0.028–10.84 /4.88	2.41–8.37 /5.64	834–1680 /1243	105.11–287.5 /166.14	2.74–8.67 /5.34	45.03–74.6 /62.48	32–218 /136	41.21–88.3 /65.13	8.0–29.36/11.24	3.27–5.46 /5.28	0.1–0.66 /0.52	0.26–0.42 /0.43
DFT-III	Pebbly fine sandstone	4.2–11.6 /4.87	0.002–0.76 /0.06	1.8–7.32 /5.72	284–648 /452	64.74–148.2 /100.24	1.96–7.2 /5.68	19.63–49.32 /36.4	13–34/23	14.63–44.9 /38.44	4.76–9.38/7.82	5.22–6.86 /6.04	0.08–0.18 /0.14	0.32–0.5 /0.46
DFT-IV	Pebbly coarse sandstone	1.4–6.16 /4.22	0.006–3.36 /0.18	0.64–2.56 /1.32	122–548 /398	81.27–126.6 /100.5	2.74–6.88 /4.7	27.2–56.34 /46.2	11–24/18	18.6–52.28 /28.7	6.7–17.65/12.2	5.12–7.31 /6.82	0.13–0.2 /0.16	0.38–0.51 /0.4
DFT-V	Fine sandstone	3.74–10.68 /6.12	0.013–6.22 /3.2	4.93–11.32 /6.34	1168–5431 /2234	88.4–224.6 /138.64	3.32–7.6 /4.88	44.28–62.76 /53.94	118–462 /188	23.18–62.16 /47.67	8.64–18.37/9.16	3.67–6.22 /5.16	0.1–0.6 /0.32	0.27–0.38 /0.34

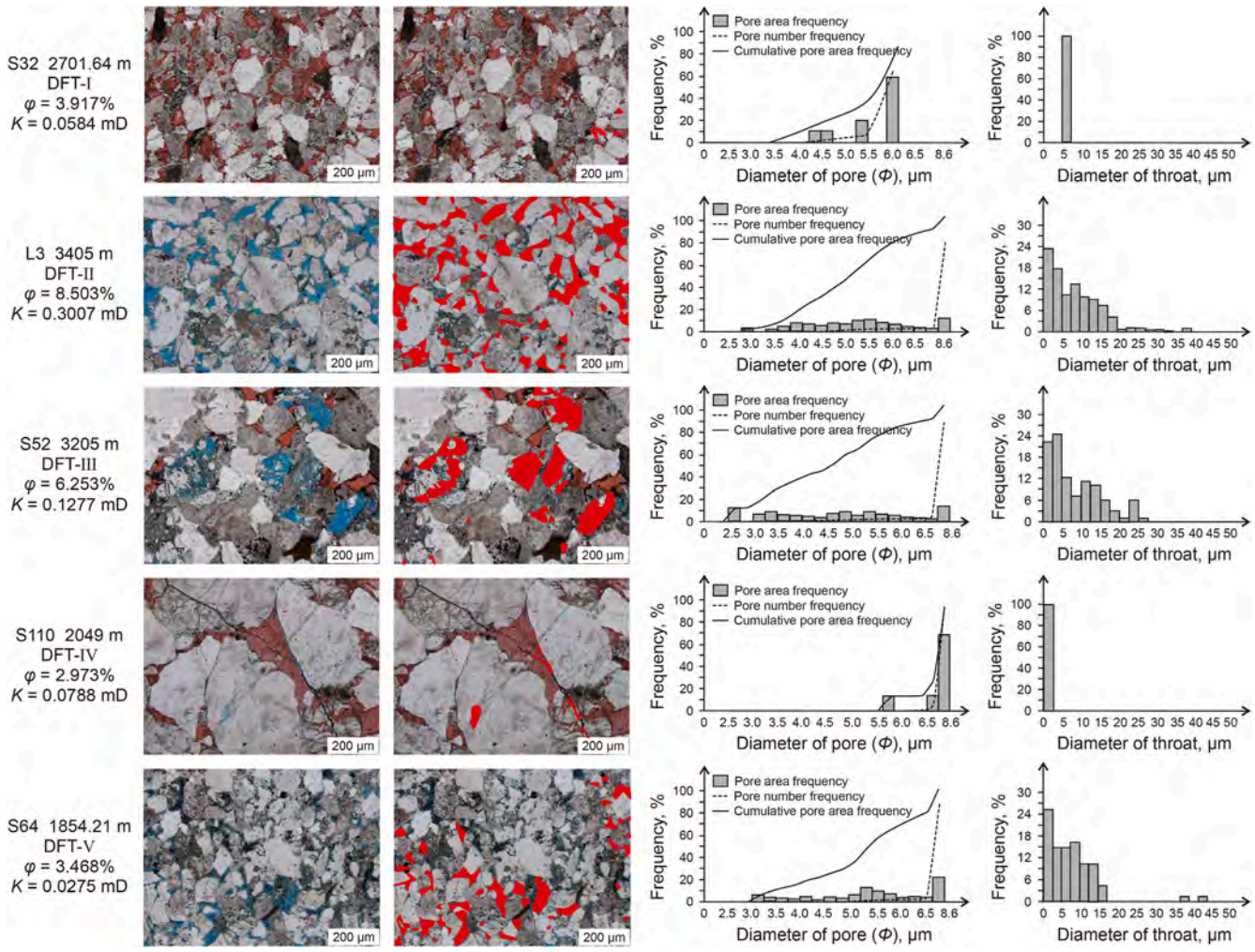


Fig. 9. Representative 2D pore-structure images and pore–throat size distributions for the five diagenetic facies.

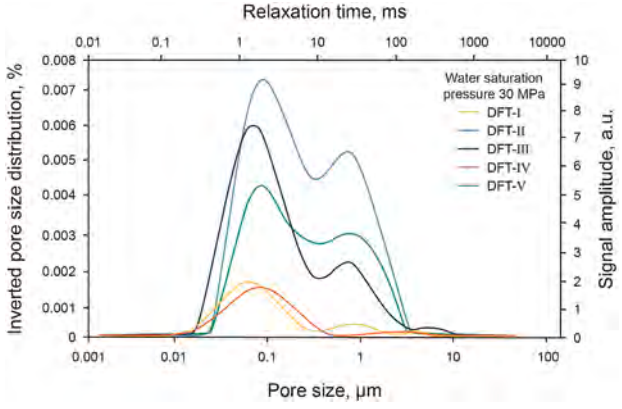


Fig. 10. NMR T_2 spectra of five diagenetic facies showing distinct pore-size distributions and fluid-storage capacities.

4.4.3. 3D pore structure characteristics of different diagenetic facies

Nuclear magnetic resonance (NMR) measurements are extensively utilized in geology to assess pore structures and fluid distribution, serving as an effective method for reservoir pore characterization (Hübner, 2014). Representative samples of the five diagenetic facies were fully saturated under a simulated formation pressure of 30 MPa and subsequently analyzed using NMR to elucidate pore structures and pore-size distributions.

As illustrated in Fig. 10, the NMR T_2 spectra reveal distinct patterns among the various facies. Facies DFT-II displays a spectrum characterized by the development of both micropores and macropores, with micropores being more predominant. Facies DFT-III exhibits a similar, albeit less pronounced, distribution, featuring well-developed micropores and relatively fewer macropores. Under conditions of weak compaction, the dissolution of carbonate cements and unstable grains significantly enhances pore development. In contrast, the spectrum of DFT-V presents an intermediate distribution, indicating moderate pore development; this suggests that even under strong compaction, dissolution may partially improve pore quality. Facies DFT-I and DFT-IV both exhibit spectra at very low levels, with only a few micropores and virtually no macropores, underscoring the severe impact of carbonate cementation on reservoir porosity.

Based on five representative diagenetic facies, five 3D pore-structure models with distinct petrophysical properties were constructed (Fig. 11). The parameters of these models are detailed in Table 4, further emphasizing the differences in pore networks among the Shahezi Formation sandstones of the northern slope of the Lishu Fault Depression. Overall, the five facies exhibit significant contrasts in porosity, permeability, and pore–throat

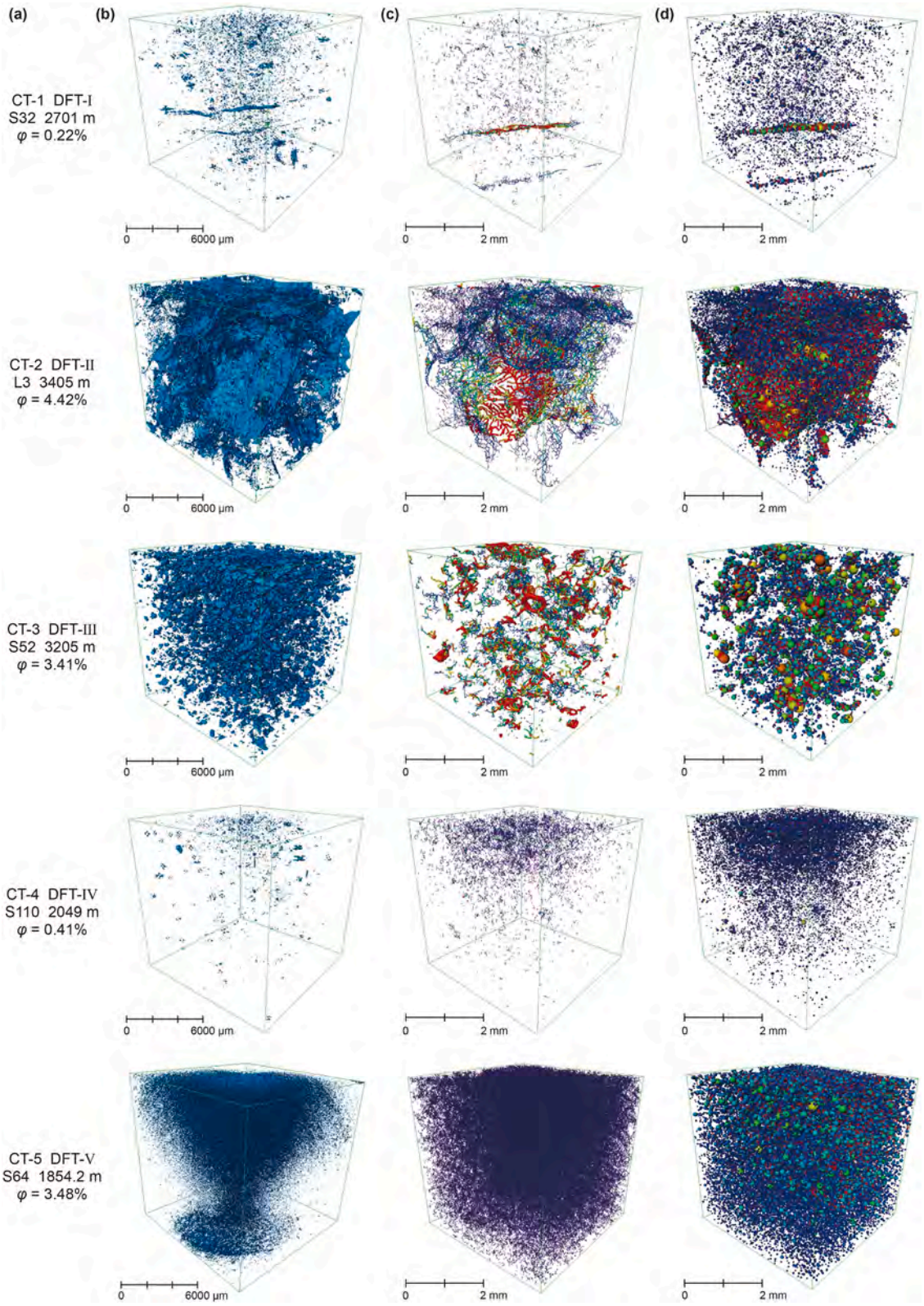


Fig. 11. Reconstructed 3D pore models demonstrating variations in pore connectivity and storage capacity among representative diagenetic facies. **(a)** Background information of the five sandstone samples; **(b)** overall pore-distribution models; **(c)** local pore-skeleton models; **(d)** local pore-network models.

Table 4
Summary of 3D pore-structure parameters for representative diagenetic facies. Abbreviations: DFT: diagenetic facies type; φ: porosity, %; K: permeability, mD; $\Phi_{averp3D}$: average 3D pore diameter, μm; $\Phi_{avert3D}$: average 3D throat diameter, μm; N_{C3D}: average 3D coordination number; N_{t3D}: total number of 3D throats.

Sample	Well	Depth, m	DFT	K, mD	φ, %	3D pore throat model			
						$\Phi_{averp3D}$, μm	$\Phi_{avert3D}$, μm	N_{C3D}	N_{t3D}
CT-1	S32	2701	DFT-I	0.0324	0.22	28.9	13.2	0.16	1302
CT-2	L3	3405	DFT-II	0.2107	4.42	32.2	21.4	1.42	17358
CT-3	S52	3205	DFT-III	0.1377	3.41	40.9	26.2	1.87	7550
CT-4	S110	2049	DFT-IV	0.0275	0.41	30.3	21.0	0.20	667
CT-5	S64	1854.2	DFT-V	0.0814	3.48	23.7	10.8	1.18	15959

connectivity, reflecting the profound influence of diagenesis on reservoir quality.

The DFT-I sample (CT-1) demonstrates extremely low porosity and permeability ($\varphi = 0.22\%$, $K = 0.0275$ mD). Its 3D pore model reveals sparse, poorly connected pores, indicating that intense compaction and cementation have obliterated nearly all primary pores, leaving only a few isolated pores and resulting in very poor reservoir quality. Conversely, the DFT-II sample (CT-2) displays the best reservoir properties, exhibiting the highest porosity and permeability ($\varphi = 4.42\%$, $K = 0.2107$ mD). Its dense and well-connected 3D pore network, characterized by the highest coordination number ($N_C = 1.87$) and throat count ($N_{t3D} = 17{,}358$), reflects a significant enhancement of pore systems through dissolution, making this the most favorable reservoir facies in the study area. The DFT-III sample (CT-3) presents moderate porosity ($\varphi = 3.41\%$) and good pore connectivity, suggesting that even under extensive compaction and cementation, moderate dissolution of feldspars and volcanic lithics effectively enhanced the pore system. In contrast, the DFT-IV sample (CT-4) exhibits extremely low porosity ($\varphi = 0.41\%$), with isolated pores and very few throats ($N_{t3D} = 667$) in the 3D model, typical of tight sandstones with negligible reservoir potential. Lastly, the DFT-V sample (CT-5) shows relatively higher porosity and permeability ($\varphi = 3.48\%$, $K = 0.1447$ mD) and a moderately developed pore network with good connectivity, indicating that secondary dissolution has partially improved pore development under compaction.

In summary, the differences in pore structures and 3D pore models indicate that reservoir quality is primarily influenced by diagenetic processes. Facies DFT-I and DFT-IV, which are subjected to significant compaction and cementation, exhibit extremely low porosity and poor connectivity, thereby categorizing them as unfavorable facies. Facies DFT-III represents an intermediate condition, reflecting the combined effects of compaction and dissolution, with reservoir quality contingent upon the local intensity of dissolution. In contrast, facies DFT-II and DFT-V demonstrate relatively high porosity and good connectivity, particularly DFT-II, which has developed the most favorable pore system due to intense dissolution. These findings suggest that facies DFT-II and DFT-V should be prioritized in the exploration of tight sandstone reservoirs on the northern slope of the Lishu Fault Depression, where they are frequently associated with high-quality source rocks and favorable structural-lithologic assemblages, thus providing substantial potential for effective reservoir development.

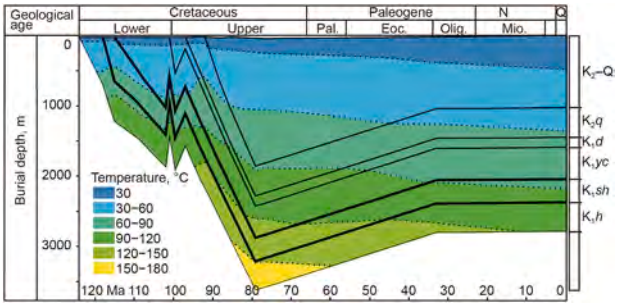


Fig. 12. Burial and thermal history curve of the Shahezi Formation sandstones on the northern slope of the Lishu Fault Depression.

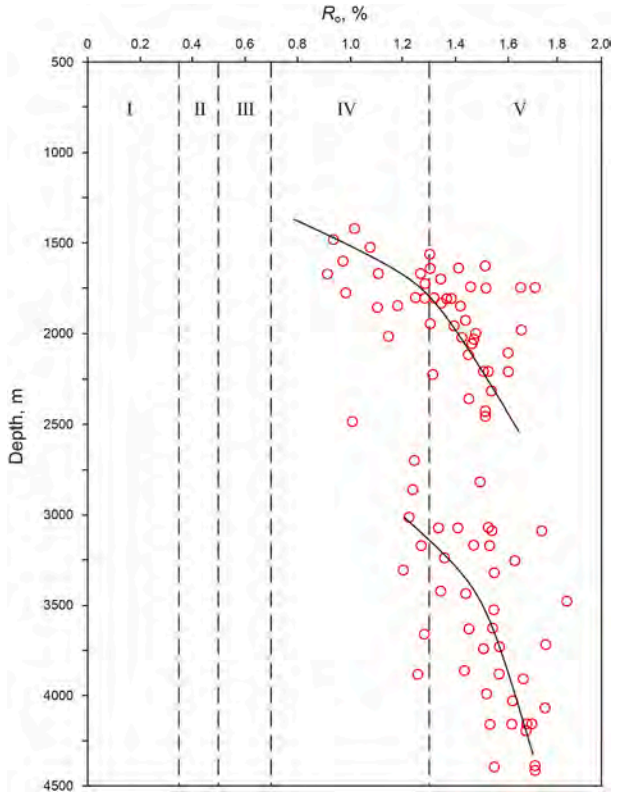


Fig. 13. Vitrinite reflectance (R_o) versus burial depth for the Shahezi Formation sandstones on the northern slope of the Lishu Fault Depression, showing the division of diagenetic stages (I–V). I = eodiagenetic stage A; II = eodiagenetic stage B; III = mesodiagenetic stage A1; IV = mesodiagenetic stage A2; V = mesodiagenetic stage B.

5. Discussion

5.1. Diagenetic evolution of the shahezi formation

Diagenetic stages represent the progressive physicochemical modifications that clastic sediments undergo after deposition and prior to metamorphism. These stages are commonly subdivided into eodiagenesis, mesodiagenesis, and telodiagenesis (Giles and Marshall, 1986; Makeen et al., 2016; Zhu et al., 2019). The classification is conventionally based on vitrinite reflectance (R_o), the smectite fraction in mixed-layer illite–smectite, paleotemperature,

and burial depth. In accordance with the Chinese national standard for clastic diagenesis (SY/T 5477-2003) and integrating petrographic, SEM, CL, and burial–thermal history evidence, the Shahezi Formation on the northern slope of the Lishu Fault Depression is interpreted to have evolved through eodiagenetic stages A and B, mesodiagenetic stage A, and currently resides in mesodiagenetic stage B (Fig. 12). Burial history modeling indicates maximum paleotemperatures of 150–180 °C, followed by a cooling phase to 90–120 °C due to late tectonic uplift. Vitrinite reflectance profiles exhibit an "isomaturity at unequal depths" pattern (Chen, 1996), reflecting differential uplift between outer-slope uplifts and inner-sag depocenters (Fig. 13).

Based on integrated core examination, blue-epoxy thin sections, CL imaging, SEM, and EDS analysis, the textures, replacement relationships, and dissolution–cementation fabrics of the Shahezi Formation sandstones were utilized to reconstruct their diagenetic evolution (Jonk et al., 2003; Xi et al., 2015). These sandstones were primarily deposited in fan-delta front settings (Wang et al., 2025). Petrographic evidence indicates that they are predominantly medium-to fine-grained sandstones with low matrix content, making them susceptible to significant mechanical compaction and early pore collapse, which established a tight reservoir framework.

During syndiagenetic to eodiagenetic stage A, mechanical compaction was the dominant process, leading to a reduction in primary intergranular porosity. The pore fluids were weakly alkaline, allowing for limited pore-filling chlorite to form in some intervals (Fig. 5(g) and (h)), while authigenic quartz was poorly developed, facilitating the partial preservation of primary pores.

In eodiagenetic stage B, meteoric water infiltration and clay-mineral reactions generated acidic fluids. Feldspar and volcanic lithics underwent dissolution, producing both intragranular and intergranular secondary pores. Feldspars were altered to kaolinite (Fig. 5(d), (g), and (j)), while localized precipitation of silica and carbonate cements occurred, imparting modest resistance to compaction (Fig. 5(i)). Primary pores continued to dominate, supplemented by limited secondary dissolution pores.

During mesodiagenetic stage A, organic matter matured, producing organic acids that further dissolved feldspar and volcanic lithics, thereby enhancing secondary porosity. The increasing burial depth and temperature accelerated clay-mineral transformation and released Fe^{2+}, Ca^{2+}, and Mg^{2+} into the pore fluids, promoting widespread carbonate cementation. In many cases, the dissolution residues of feldspar and lithics were replaced by calcite cement (Fig. 5(d)).

During the mesodiagenetic stage B, residual organic acids continued to generate dissolution pores, while secondary quartz overgrowths were observed in some samples (Fig. 5(a)). In others, authigenic illite filled secondary pores (Fig. 5(l)), thereby reducing reservoir quality. The alkaline conditions of the pore fluid facilitated the precipitation of ferroan calcite and ferroan dolomite (Fig. 5(f)), which occluded the remaining intergranular pores and resulted in the formation of very tight reservoir intervals. The evolution of burial temperature, the transformation from smectite to illite, and the dissolution textures caused by organic acids, as observed in SEM and XRD analyses, collectively support this diagenetic evolution model (Figs. 5 and 12–14).

5.2. Different influences of diagenetic factors on reservoir quality

Diagenesis encompasses all physical, chemical, and biochemical processes that affect sediments after deposition and prior to metamorphism, reflecting the evolving conditions of burial and fluid flow over geological time (de Segonzac, 1968; Zou et al., 2008; Yang et al., 2018). In tight gas sandstones, the predominant diagenetic processes include compaction, cementation, replacement, and dissolution. These processes occur within various diagenetic environments, generating distinct mineral assemblages and pore structure characteristics, which ultimately lead to significant variations in reservoir quality (Lai et al., 2017; Li et al., 2018).

Mechanical compaction and chemical pressure solution progressively reduce porosity by tightening grain packing and dissolving grain contacts. These processes are influenced by detrital composition, grain texture, burial depth, diagenetic stage, and pore-fluid pressure (Enayati-Bidgoli and Saemi, 2019). As burial progresses, grains become tightly packed, indented, and fractured, resulting in significant porosity loss (Xu et al., 2001; Ajdukiewicz et al., 2010). Diagnostic features of mechanical compaction include grain-contact styles, grain alignment, and the differential fracturing of brittle minerals (e.g., quartz) compared to plastic minerals (e.g., micas, mud clasts) (Lai et al., 2016). Cementation involves the precipitation of authigenic minerals that occlude pores and bind detrital grains. Quartz overgrowths, carbonate cementation, and clay-mineral precipitation often impair pore connectivity, with their effects strongly dependent on timing and mineralogy (Morad et al., 2010; Lai et al., 2018). Replacement reactions, such as the transformation of feldspar into kaolinite or carbonate, may alter mineralogy without significantly affecting intergranular volume (Amireh, 2020). Dissolution, driven by organic acids, meteoric fluids, and burial diagenesis, generates secondary porosity but does not fully compensate for the porosity loss associated with progressive burial (Ehrenberg, 1990; Lima and De Ros, 2002). In tight sandstones, the dissolution of feldspar, volcanic lithics, and carbonate cement serves as a key mechanism for the formation of 'sweet spot' reservoirs.

5.2.1. Mechanical compaction and cementation

Mechanical compaction and cementation exert the most significant influence on pore evolution in the Shahezi Formation. Intergranular volume–cementation cross-plots (Houseknecht, 1987; Haile et al., 2019) for 61 samples from five wells (Fig. 15) indicate that both processes considerably reduce porosity and permeability. As cementation leads to an increase in porosity loss, the intergranular volume may locally increase, suggesting that cementation can both compromise pore space and maintain framework stability during the early stages. In contrast, the systematic decrease in intergranular volume due to increasing porosity loss from compaction confirms its predominant destructive role.

Compaction intensity generally escalates with burial depth. Although a negative porosity–depth trend is anticipated (Fig. 16), variations in sediment supply and dissolution processes locally alter this relationship (Taylor, 1990). Overall, mechanical compaction serves as the primary control on reservoir densification within the Shahezi Formation, while cementation functions as an additional, albeit variably destructive, factor.

5.2.2. Influences of carbonate cementation

Carbonate cementation is a significant factor contributing to reservoir deterioration in deep tight sandstones (Fig. 15). The carbon and oxygen isotope ratios from five cored wells (Fig. 17) indicate that carbonate precipitation in the Shahezi Formation is primarily linked to diagenetic reactions and the decarboxylation of organic matter. During the early burial stages, lacustrine biochemical precipitation and iron-rich fluids resulting from clay-mineral transformation led to the formation of early calcite and ferroan calcite cementation. In the mid-burial diagenesis phase, the degradation of organic matter released Ca^{2+} ions that migrated through pore networks, precipitating as carbonate cement. In

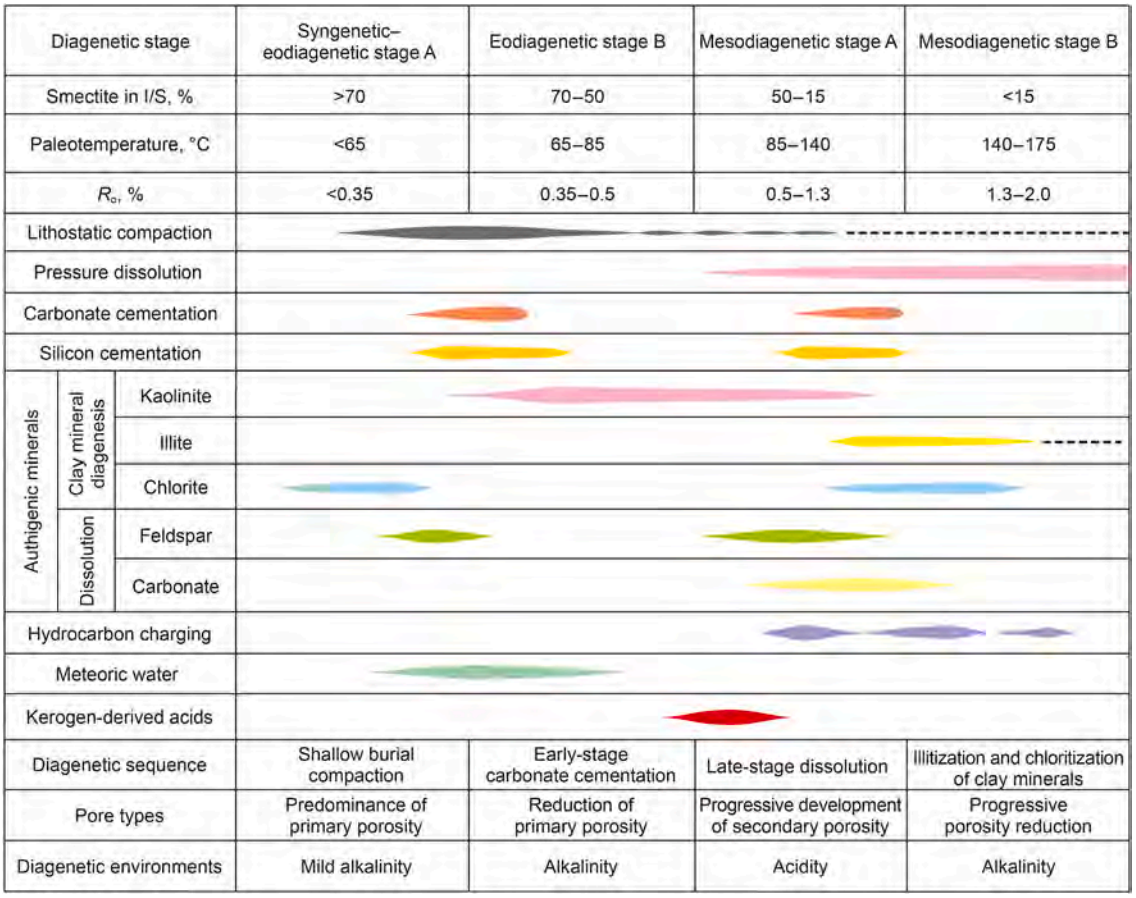


Fig. 14. Schematic diagenetic evolution sequence of the Shahezi Formation sandstones on the northern slope of the Lishu Fault Depression.

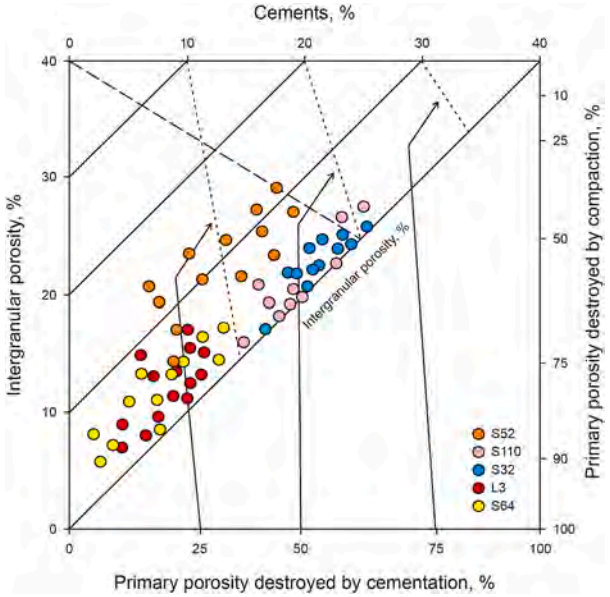


Fig. 15. Intergranular porosity–cementation cross-plot for the Shahezi Formation sandstones, showing quantitative effects of mechanical compaction and cementation on primary porosity reduction.

deeper burial environments, hydrocarbon-sulfate reactions produced H_2S and diagenetic carbonates, while volcanic-derived iron supplied ferroan calcite, further diminishing porosity. Localized dissolution by organic acids during mesodiagenesis partially reversed early pore occlusion, creating intragranular and intergranular dissolution pores and establishing limited but effective fluid flow pathways. Consequently, the deep Shahezi reservoirs are the result of a dynamic balance between destructive carbonate cementation and constructive organic-acid dissolution.

5.2.3. *Effects of volcaniclastic input on reservoir quality*

Volcaniclastic input exerts a unique multi-stage control over diagenesis and pore evolution in the Shahezi Formation. Fresh volcanic lithics and glass shards are thermodynamically unstable due to their amorphous structure, high surface energy, and metastable mineralogy (e.g., glass, feldspathoids, and pyroxenes). Their alteration rapidly releases labile cations (Ca^{2+}, Mg^{2+}, Fe^{2+}, Na^{+}, K^{+}), thereby promoting early carbonate and clay-mineral cementation, which accelerates the loss of primary porosity. This observation aligns with the widespread development of calcite, ferroan calcite, and illite in the study area.

Simultaneously, the alteration of volcanic components and the maturation of organic matter generate acidic fluids enriched in H^{+} and complexing ligands, which facilitate the dissolution of feldspar and volcanic lithics. This process results in the production of abundant secondary porosity and locally enhances permeability. The coupled dissolution–cementation mechanism leads to highly heterogeneous pore systems, characterized by zones enriched in dissolution alternating with tightly cemented intervals. Similar volcaniclastic-driven diagenetic feedbacks have been documented globally (Ding et al., 2020; Weibel et al., 2023; Zhang et al., 2024).

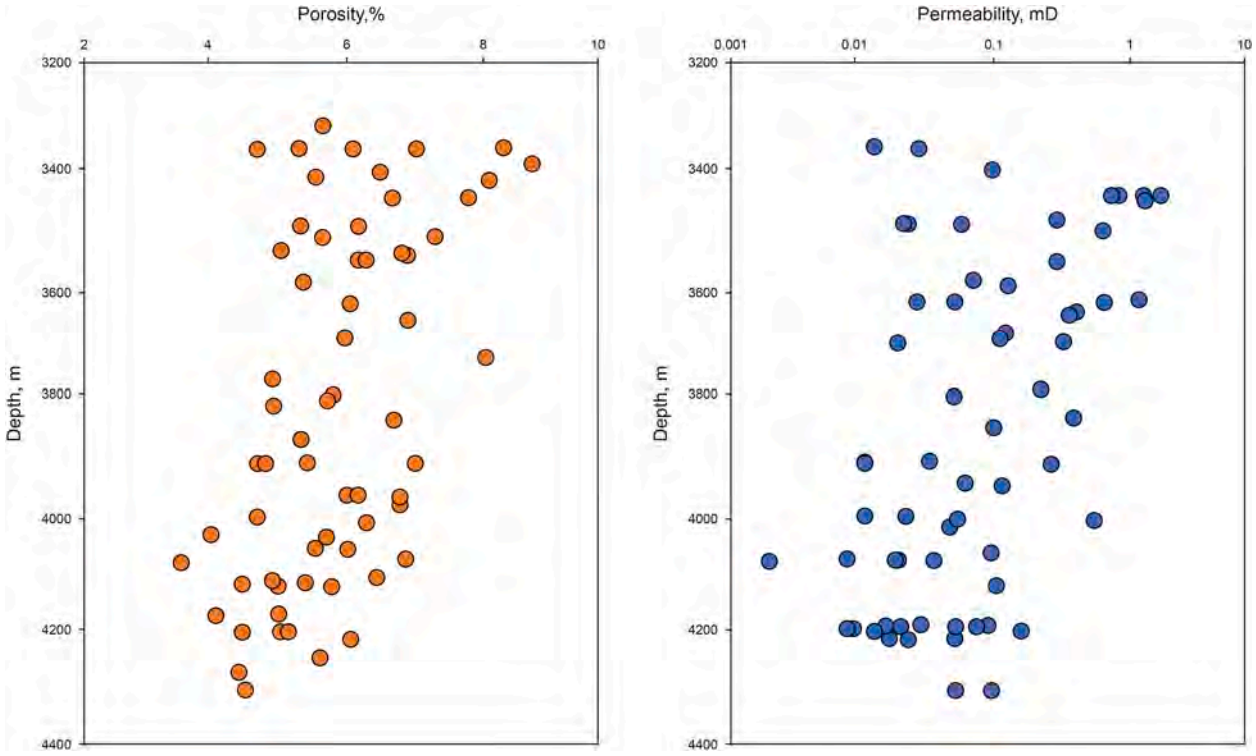


Fig. 16. Depth–porosity–permeability relationships for the Shahezi Formation sandstones. Overall porosity decreases with burial depth, but deviations from the normal compaction trend reflect localized dissolution and variable sediment supply, influencing pore preservation in deep lacustrine rift settings.

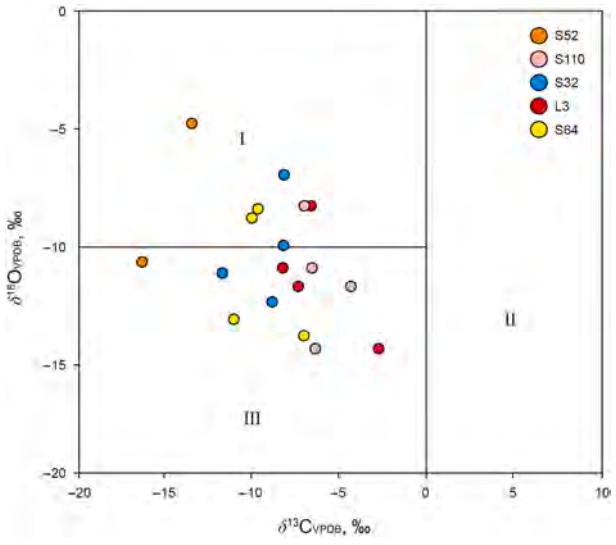


Fig. 17. Cross-plot of carbon and oxygen isotope values for carbonate cements from the Shahezi Formation. Most data fall within diagenetic and organic-matter decarboxylation fields, indicating mixed carbonate sources including early pore-fluid precipitation, organic-acid dissolution–reprecipitation, and late ferroan cementation.

Additionally, quartz dissolution and silica re-precipitation observed in this study (consistent with Liu et al., 2025) further substantiate acid-mediated reactions in volcaniclastic reservoirs. Overall, the supply of volcaniclastic material fundamentally governs pore-fluid chemistry, mineral reactions, and the spatial distribution of high-quality reservoirs in the Shahezi Formation.

5.3. Formation mechanism of various diagenetic facies types

Even within the same depositional facies, variations in diagenetic processes and evolutionary pathways can lead to reservoirs with highly heterogeneous pore architectures and petrophysical properties. Since diagenetic facies are fundamentally linked to diagenetic evolution, the mechanisms governing their development serve as primary controls on the spatial distribution and heterogeneity of tight sandstone reservoirs (Lai et al., 2017; Zhu et al., 2020). In deeply buried tight reservoirs, such as those in the Shahezi Formation, diagenetic processes—including compaction, cementation, and dissolution—dictate pore-system evolution and fluid flow capacity. A robust identification of diagenetic facies and an interpretation of the underlying genetic mechanisms not only enhance understanding of diagenetic evolution but also provide a predictive basis for identifying high-quality reservoir intervals.

Based on blue-epoxy thin sections and pore-type observations, this study defines five diagenetic facies, discussing their formation mechanisms, pore-evolution pathways, and characteristic petrographic signatures (Fig. 18). Unlike purely siliciclastic tight sandstones, where porosity reduction is primarily driven by mechanical compaction and silica cementation, volcaniclastic-rich systems experience a dual diagenetic regime characterized by initial cation-rich fluids followed by later acidic fluid pulses resulting from volcaniclastic alteration. This coupled cementation-dissolution system leads to more complex pore-evolution trajectories and increased reservoir heterogeneity, highlighting the necessity of employing a diagenetic facies scheme specifically designed for volcaniclastic reservoirs. To elucidate the diagenetic evolution patterns for each facies, the following section presents a

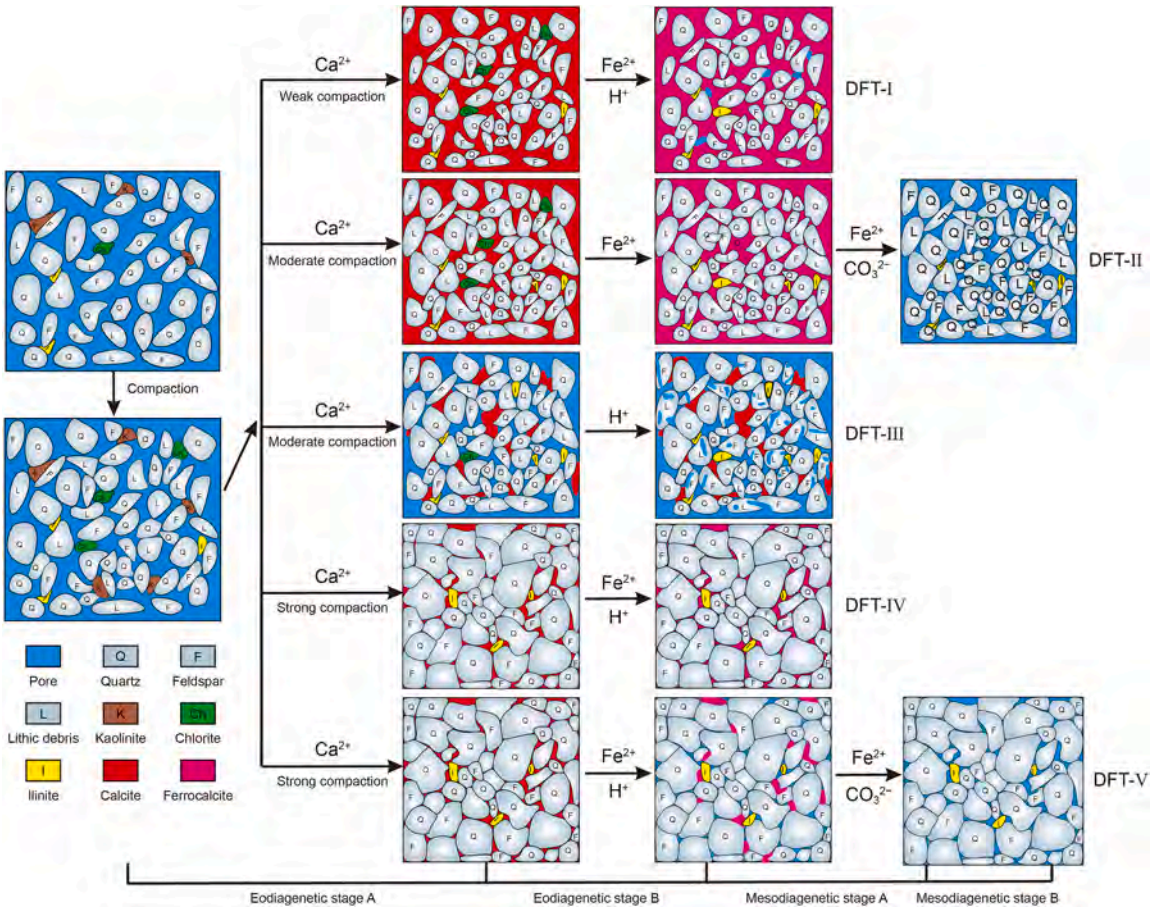


Fig. 18. Conceptual diagenetic evolution model for the Shahezi Formation tight sandstones on the northern slope of the Lishu Fault Depression.

facies-by-facies assessment that integrates petrographic, CL, SEM, NMR, and CT evidence.

5.3.1. Tightly cemented diagenetic facies (DFT-I)

DFT-I is characterized by pervasive carbonate cementation, with calcite and ferroan calcite nearly occluding intergranular pores (Fig. 7(a)). Local feldspar grains are replaced by calcite. The styles of grain contact and close packing indicate strong mechanical compaction. This facies formed during early to mesodiagenesis under relatively closed fluid systems with limited fluid throughput. The carbonate cements likely originated from compactional expulsion or Ca-rich fluids resulting from the dissolution of overlying carbonates. The reservoir quality is extremely poor, and only later-stage dissolution can locally enhance porosity.

5.3.2. Moderately compacted, carbonate-dissolution facies (DFT-II)

DFT-II is distinguished by the partial dissolution of early carbonate cements, which generates intragranular dissolution pores and microfractures (Fig. 7(b)). Compaction is moderate, and the distribution of carbonate cement is heterogeneous. This formation occurred during mesodiagenesis, when organic-acid generation from source-rock maturation facilitated the dissolution of early carbonates, thereby improving pore connectivity. NMR and petrophysical data confirm that DFT-II exhibits the most favorable reservoir quality (Figs. 8–10).

5.3.3. Moderately compacted, unstable-grain dissolution facies (DFT-III)

DFT-III demonstrates extensive dissolution of volcanic lithics and feldspars, resulting in abundant secondary intragranular pores (Fig. 7(c)). Moderate compaction and localized clay cementation are present. This facies is the result of deep-burial acidic fluids derived from organic acids and clay mineral reactions. Secondary pores are occasionally occluded by subsequent clay or ferruginous cement, reflecting episodic fluid events. The reservoir properties are favorable, ranking second to DFT-II.

5.3.4. Strongly compacted, densely cemented facies (DFT-IV)

DFT-IV facies is characterized by intense mechanical compaction, which results in the presence of only isolated residual pores that were subsequently infilled by late-stage calcite (see Fig. 7(d)). The grain contacts within this facies vary from linear to sutured, with minimal dissolution observed due to restricted fluid access. This facies exemplifies an end-member densification pathway that is driven by progressive burial and limited early cement shielding. Consequently, the reservoir quality of this facies is negligible.

5.3.5. Strongly compacted, intergranular-dissolution facies (DFT-V)

DFT-V facies has experienced strong compaction akin to DFT-IV; however, the later introduction of acidic fluids has led to the development of secondary intergranular dissolution pores (refer to Fig. 7(e)). Thin clay coatings and relatively weak late cementation have preserved limited permeability pathways. While the porosity in

DFT-V is greater than that in DFT-IV, the poor connectivity of the pores results in moderate reservoir quality, which is ranked below that of DFT-II and DFT-III.

5.3.6. Synthesis

Although each facies exhibits distinct diagenetic pathways and reservoir behaviors, they are fundamentally governed by the regional burial–thermal history (Fig. 12). Deep burial (4000 m) and elevated formation temperatures (160 °C) facilitated the evolution of clay from smectite/kaolinite to illite (Yu et al., 2019), which is consistent with advanced mesodiagenesis. The absence of chlorite indicates a limited supply of Fe–Mg and contrasts with Fe-rich settings such as the Xihu Sag of the East China Sea Shelf Basin (Zhao et al., 2022). The low abundance of kaolinite in deeper intervals suggests burial beyond the 'kaolinite death depth', which aligns with the dominance of illitization.

Importantly, the Shahezi system fundamentally differs from purely siliciclastic tight sandstones. The presence of volcanic lithics and glass provided early Ca–Mg–Fe ions and subsequently acidic fluids, driving alternating phases of cementation and dissolution. This volcaniclastic-mediated fluid–rock interaction resulted in greater heterogeneity and more complex reservoir quality patterns, underscoring the critical role of sediment provenance in diagenetic evolution.

6. Conclusions

1) Five diagenetic facies were identified in the tight sandstones of the Shahezi Formation on the northern slope of the Lishu Fault Depression, reflecting systematic variations in compaction, cementation, and dissolution. These facies demonstrate distinct pore-evolution pathways and reservoir quality, influenced by fluid–rock interactions and diagenetic timing.
2) Integrated digital image analysis, NMR, and micro-CT investigations reveal significant differences in pore architecture among the facies. DFT-II and DFT-V, characterized by dissolution-enhanced pore development and improved throat connectivity, represent the most favorable reservoir types. In contrast, DFT-I and DFT-IV exhibit intense compaction and pervasive cementation, resulting in ultra-tight intervals. The porosity–permeability relationships suggest a similar detrital provenance but indicate that strong diagenetic overprinting is the primary control on reservoir quality.
3) The diagenetic evolution ranges from syndiagenesis to advanced mesodiagenesis, encompassing early mechanical compaction, meteoric- and organic-acid-driven dissolution, and late ferroan carbonate precipitation. Dissolution plays a crucial constructive role by generating secondary porosity; however, its effects are counterbalanced by compaction and cementation, leading to heterogeneous pore systems.
4) The diagenetic–pore system framework established in this study enhances the understanding of reservoir heterogeneity in volcaniclastic-rich tight sandstones and provides a predictive basis for identifying high-quality intervals in deeply buried rift-basin settings. Although this study relies on natural core samples and multi-scale imaging, the lack of controlled fluid–rock reaction experiments and kinetic constraints limits the quantitative assessment of volcaniclastic dissolution processes. Future research will incorporate hydrothermal experiments and numerical simulations to refine reaction pathways and quantify porosity evolution associated with volcaniclastic input.

CRediT authorship contribution statement

Shu-Yang Wang: Writing – review & editing, Writing – original draft, Validation, Software, Formal analysis, Data curation. **Xuan-Long Shan:** Writing – review & editing, Visualization, Resources. **Chao-Fan Zhu:** Visualization, Methodology, Formal analysis. **Wen-Tong He:** Writing – review & editing, Methodology, Funding acquisition. **Yi-Bo Wang:** Software, Conceptualization. **Ying Bian:** Validation, Supervision. **Yu-Feng Shen:** Methodology. **Nan Jiang:** Formal analysis. **Xin-Tao Ma:** Validation. **Ze-Yu Ji:** Investigation. **Qi-Xian Xie:** Formal analysis. **De-Kun Zhu:** Visualization.

Declaration of competing interest

The authors declare no conflicts of interest.

Acknowledgements

This research was supported by the National Natural Science Foundation of China (Grant No. 42402167) and the Special Fund of the State Key Laboratory of Deep Earth Exploration and Imaging (Grant No. DEEI20251244).

References

Ajdukiewicz, J.M., Nicholson, P.H., Esch, W.L., 2010. Prediction of deep reservoir quality using early diagenetic process models in the Jurassic Norphlet Formation, Gulf of Mexico. AAPG Bull. 94 (8), 1189–1227. https://doi.org/10.1306/04211009152.

Al-Juboury, A., Howard, J.P., Vincent, S.J., et al., 2021. Petrography, diagenesis and geochemistry of the Cambro–Ordovician Khabour sandstones, Western Iraq: Implications for reservoir quality and the impact of the Hirnantian glaciation. Mar. Petrol. Geol. 123, 104733. https://doi.org/10.1016/j.marpetgeo.2020.104733.

Amireh, B.S., 2020. Weathering, recycling, hydraulic sorting and metamorphism/metasomatism implications of the NE Gondwana Lower Cambrian–Lower Cretaceous siliciclastic succession of Jordan. J. Asian Earth Sci. 191, 104228. https://doi.org/10.1016/j.jseaes.2020.104228.

Arvidson, R., Mackenzie, F., 1999. The dolomite problem: Control of precipitation kinetics by temperature and saturation state. Am. J. Sci. 299 (4), 257–288. https://doi.org/10.2475/ajs.299.4.257.

Bai, Y., Sun, W., Ren, D., et al., 2018. Quantitative classification and characteristic difference of diagenetic facies in He 8 reservoir of the Su 48 block, west area of Sulige Gas Field, Ordos Basin. Nat. Gas Geosci. 29 (12), 1739–1747. https://doi.org/10.11764/j.issn.1672-1926.2018.08.002 (in Chinese).

Baudon, C., Fabuel-Perez, I., Redfern, J., 2009. Structural style and evolution of a Late Triassic rift basin in the central high atlas, Morocco: Controls on sediment deposition. Geol. J. 44 (6), 677–691. https://doi.org/10.1002/gj.1195.

Bosworth, W., 1985. Geometry of propagating continental rifts. Nature 316 (6029), 625–627. https://doi.org/10.1038/316625a0.

Cao, H., He, W., 2020. Correlation of carbon isotope stratigraphy and paleoenvironmental conditions in the Cretaceous Jehol Group, northeastern China. Int. Geol. Rev. 62 (1), 113–128. https://doi.org/10.1080/00206814.2019.1681303.

Chen, D., 1996. Structural setting for "shallow" maturation of the lower tertiary source rocks in Subei Basin, China. Petrol. Explor. Dev. 23 (4), 6–10 (in Chinese).

Coplen, T.B., Brand, W.A., Gehre, M., et al., 2006. New guidelines for $\delta^{13}C$ measurements. Anal. Chem. 78 (7), 2439–2441. https://doi.org/10.1021/ac052027c.

Critelli, S., Muto, F., Perri, F., et al., 2017. Interpreting provenance relations from sandstone detrital modes, southern Italy foreland region: Stratigraphic record of the Miocene tectonic evolution. Mar. Petrol. Geol. 87, 47–59. https://doi.org/10.1016/j.marpetgeo.2017.01.026.

de Segonzac, G.D., 1968. The birth and development of the concept of diagenesis (1866–1966). Earth Sci. Rev. 4, 153–201. https://doi.org/10.1016/0012-8252(68)90149-9.

Ding, C., Pang, Y.Q., Meng, Y.L., et al., 2020. Study of the paleoenvironment and reservoir mechanism for volcanic rich clastic reservoirs in the upper Urho Formation in the Zhongguai Region, Junggar Basin. Acta Sedimentol. Sin. 38 (4), 851–867. https://doi.org/10.14027/j.issn.1000-0550.2020.054 (in Chinese).

Du, S., Zhao, Y., Jin, J., et al., 2019. Significance of the secondary pores in perthite for oil storage and flow in tight sandstone reservoir. Mar. Petrol. Geol. 110, 178–188. https://doi.org/10.1016/j.marpetgeo.2019.07.006.

Ehrenberg, S.N., 1990. Relationship between diagenesis and reservoir quality in sandstones of the Garn Formation, Haltenbanken, Mid-Norwegian continental

shelf. AAPG Bull. 74 (10), 1538–1558. https://doi.org/10.1306/0C9B2515-1710-11D7-8645000102C1865D.
Enayati-Bidgoli, A., Saemi, E., 2019. Effects of late diagenesis on primary reservoir quality of a quartz arenite unit: A case study from the Lower Cretaceous successions of SW Iran. Petrol. Sci. 16 (2), 267–284. https://doi.org/10.1007/s12182-019-0306-x.
Feng, Y., Jiang, S., Wang, C., 2015. Sequence stratigraphy, sedimentary systems and petroleum plays in a low-accommodation basin: Middle to upper members of the Lower Jurassic Sangonghe Formation, Central Junggar Basin, Northwestern China. J. Asian Earth Sci. 105, 85–103. https://doi.org/10.1016/j.jseaes.2015.03.025.
Feng, Z.Q., Liu, J., Wang, P.J., et al., 2011. New oil and gas exploration field: Volcanic hydrocarbon reservoirs: Enlightenment from the discovery of the large gas field in Songliao Basin. Chin. J. Geophys. 54 (2), 269–279. https://doi.org/10.3969/j.issn.0001-5733.2011.02.001 (in Chinese).
Folk, R.L., Andrews, P.B., Lewis, D.W., 1970. Detrital sedimentary rock classification and nomenclature for use in New Zealand. N. Z. J. Geol. Geophys. 13 (4), 937–968. https://doi.org/10.1080/00288306.1970.10418211.
Gao, Y., Wang, C., Liu, Z., et al., 2015. Diagenetic and paleoenvironmental controls on Late Cretaceous clay minerals in the Songliao Basin, Northeast China. Clays Clay Miner. 63 (6), 469–484. https://doi.org/10.1346/CCMN.2015.0630605.
Giles, M.R., Marshall, J.D., 1986. Constraints on the development of secondary porosity in the subsurface: Re-evaluation of processes. Mar. Petrol. Geol. 3 (3), 243–255. https://doi.org/10.1016/0264-8172(86)90048-6.
Gupta, S., Cowie, P.A., Dawers, N.H., et al., 1998. A mechanism to explain rift-basin subsidence and stratigraphic patterns through fault-array evolution. Geology 26 (7), 595. https://doi.org/10.1130/0091-7613(1998)026<0595:AMTERB2.3.CO;2.
Haile, B.G., Czarniecka, U., Xi, K., et al., 2019. Hydrothermally induced diagenesis: Evidence from shallow marine-deltaic sediments, Wilhelmøya, Svalbard. Geosci. Front. 10 (2), 629–649. https://doi.org/10.1016/j.gsf.2018.02.015.
Hasnan, H.K., Sheppard, A., Hassan, M.H.A., et al., 2020. Digital core analysis: Characterizing reservoir quality through thin sandstone layers in heterolithic rocks. J. Appl. Geophys. 182, 104178. https://doi.org/10.1016/j.jappgeo.2020.104178.
Hong, D., Cao, J., Wu, T., et al., 2020. Authigenic clay minerals and calcite dissolution influence reservoir quality in tight sandstones: Insights from the central Junggar Basin, NW China. Energy Geosci 1 (1–2), 8–19. https://doi.org/10.1016/j.engeos.2020.03.001.
Hou, Q., Zhao, Z., Huang, Z., 2011. Accumulation threshold and exploration potential of deep basin oil in the Songliao Basin. Petrol. Explor. Dev. 38 (5), 523–529. https://doi.org/10.1016/S1876-3804(11)60052-9.
Houseknecht, D.W., 1987. Assessing the relative importance of compaction processes and cementation to reduction of porosity in sandstones. AAPG Bull. 71 (6), 633–642. https://doi.org/10.1306/9488787F-1704-11D7-8645000102C1865D.
Hu, W.S., Lü, B.Q., Zhang, W.J., et al., 2005. An approach to tectonic evolution and dynamics of the Songliao Basin. Chin. J. Geol. 40 (1), 16–31 (in Chinese).
Hübner, W., 2014. Studying the pore space of cuttings by NMR and μCT. J. Appl. Geophys. 104, 97–105. https://doi.org/10.1016/j.jappgeo.2014.02.016.
Jabir, A., Cerepi, A., Loisy, C., et al., 2021. Evaluation of reservoir systems in Paleozoic sedimentary formations of Ghadames and Jefarah basins. J. Afr. Earth Sci. 183, 104324. https://doi.org/10.1016/j.jafrearsci.2021.104324.
Jonk, R., Duranti, D., Parnell, J., et al., 2003. The structural and diagenetic evolution of injected sandstones: Examples from the Kimmeridgian of NE Scotland. J. Geol. Soc. 160 (6), 881–894. https://doi.org/10.1144/0016-764902-091.
Lai, J., Wang, G., Chai, Y., et al., 2017. Deep burial diagenesis and reservoir quality evolution of high-temperature, high-pressure sandstones: Examples from Lower Cretaceous Bashijiqike Formation in Keshen area, Kuqa Depression, Tarim Basin of China. AAPG Bull. 101 (6), 829–862. https://doi.org/10.1306/08231614008.
Lai, J., Wang, G., Ran, Y., et al., 2016. Impact of diagenesis on the reservoir quality of tight oil sandstones: The case of Upper Triassic Yanchang Formation Chang 7 oil layers in Ordos Basin, China. J. Petrol. Sci. Eng. 145, 54–65. https://doi.org/10.1016/j.petrol.2016.03.009.
Lai, J., Wang, G., Wang, S., et al., 2018. Review of diagenetic facies in tight sandstones: Diagenesis, diagenetic minerals, and prediction via well logs. Earth Sci. Rev. 185, 234–258. https://doi.org/10.1016/j.earscirev.2018.06.009.
Li, P., Sun, W., Gao, Y., et al., 2018. Quantitative calculation of tight sandstone reservoir porosity evolution based on different diagenesis: A case study from Chang 81 reservoir of Maling area, Ordos Basin. Geol. Sci. Technol. Inf. 37 (1), 135–142 (in Chinese).
Lima, R.D., De Ros, L.F., 2002. The role of depositional setting and diagenesis on the reservoir quality of Devonian sandstones from the Solimões Basin, Brazilian Amazonia. Mar. Petrol. Geol. 19 (9), 1047–1071. https://doi.org/10.1016/S0264-8172(03)00002-3.
Liu, K.X., Wang, J.H., Yin, G.F., et al., 2025. Quartz dissolution and its mechanisms in the Pinghu Formation, Baowu area, Xihu Sag, East China Sea Shelf Basin. Oil Gas Geol. 46 (4), 1349–1366. https://doi.org/10.11743/ogg20250421.
Liu, L., Li, Y., Dong, H., et al., 2020. Diagenesis and reservoir quality of Paleocene tight sandstones, Lishui Sag, East China Sea Shelf Basin. J. Petrol. Sci. Eng. 195, 107615. https://doi.org/10.1016/j.petrol.2020.107615.
Makeen, Y.M., Abdullah, W.H., Ayinla, H.A., et al., 2016. Sedimentology, diagenesis and reservoir quality of the upper Abu Gabra Formation sandstones in the Fula Sub-basin, Muglad Basin, Sudan. Mar. Petrol. Geol. 77, 1227–1242. https://doi.org/10.1016/j.marpetgeo.2016.08.015.
Morad, S., Al-Ramadan, K., Ketzer, J.M., et al., 2010. The impact of diagenesis on the heterogeneity of sandstone reservoirs: A review of the role of depositional facies and sequence stratigraphy. AAPG Bull. 94 (8), 1267–1309. https://doi.org/10.1306/04211009178.
Pettijohn, F.J., Potter, P.E., Siever, R., 1987. Sand and Sandstone. Springer, New York, New York. https://doi.org/10.1007/978-1-4612-1066-5.
Prosser, S., 1993. Rift-related linked depositional systems and their seismic expression. Geol. Soc. Lond. Spec. Publ. 71, 35–66. https://doi.org/10.1144/GSL.SP.1993.071.01.03.
Qiao, J., Zeng, J., Jiang, S., et al., 2020. Impacts of sedimentology and diagenesis on pore structure and reservoir quality in tight oil sandstone reservoirs: Implications for macroscopic and microscopic heterogeneities. Mar. Petrol. Geol. 111, 279–300. https://doi.org/10.1016/j.marpetgeo.2019.08.008.
Santosh, M., Feng, Z.Q., 2020. New horizons in energy geoscience. Energy Geosci 1 (1–2), A1. https://doi.org/10.1016/j.engeos.2020.05.005.
Schlüter, S., Sheppard, A., Brown, K., et al., 2014. Image processing of multiphase images obtained via X-ray microtomography: A review. Water Resour. Res. 50 (4), 3615–3639. https://doi.org/10.1002/2014WR015256.
Song, X.F., Wei, H.R., Li, W.J., et al., 2022. Evaluation on influencing factors of water lock damage of tight sandstone gas reservoir in Block M of Tarim Basin. Fault-Block Oil Gas Field 29 (2), 224–228 (in Chinese).
Spötl, C., 2011. Long-term performance of the Gasbench isotope ratio mass spectrometry system for the stable isotope analysis of carbonate microsamples. Rapid Commun. Mass Spectrom. 25 (11), 1683–1685. https://doi.org/10.1002/rcm.5037.
Su, Y., Zha, M., Jiang, L., et al., 2022. Pore structure and fluid distribution of tight sandstone by the combined use of SEM, MICP and X-ray micro-CT. J. Petrol. Sci. Eng. 208, 109241. https://doi.org/10.1016/j.petrol.2021.109241.
Taylor, T.R., 1990. The influence of calcite dissolution on reservoir porosity in Miocene sandstones, Picaroon Field, offshore Texas Gulf Coast. J. Sediment. Res. 60 (3), 322–334. https://doi.org/10.1306/212F9192-2B24-11D7-8648000102C1865D.
Wang, C., Lyu, Y., Wang, Q., et al., 2017. Evaluations of oil and gas lateral migration across faults: A case study of Shigezhuang nose structure of Wen'an slope in Baxian Sag, Jizhong Depression, Bohai Bay Basin, East China. Petrol. Explor. Dev. 44 (6), 932–940. https://doi.org/10.1016/S1876-3804(17)30105-2.
Wang, H., Fan, T., Wu, Y., 2015. The subsurface structure and stratigraphic architecture of rift-related units in the Lishu Depression of the Songliao Basin, China. J. Asian Earth Sci. 99, 13–29. https://doi.org/10.1016/j.jseaes.2014.11.026.
Wang, S., Shan, X., Yang, Q., et al., 2025. Tight gas accumulation in middle to deep successions of fault depression slopes: Northern slope of the Lishu Depression, Songliao Basin. Mar. Petrol. Geol. 174, 107302. https://doi.org/10.1016/j.marpetgeo.2025.107302.
Wang, Z., Luo, X., Lei, Y., et al., 2020. Impact of detrital composition and diagenesis on the heterogeneity and quality of low-permeability to tight sandstone reservoirs: An example of the Upper Triassic Yanchang Formation in southeastern Ordos Basin. J. Petrol. Sci. Eng. 195, 107596. https://doi.org/10.1016/j.petrol.2020.107596.
Weibel, R., Nielsen, M.T., Therkelsen, J., et al., 2020. Illite distribution and morphology explaining basinal variations in reservoir properties of Upper Jurassic sandstones, Danish North Sea. Mar. Petrol. Geol. 116, 104290. https://doi.org/10.1016/j.marpetgeo.2020.104290.
Weibel, R., Vosgerau, H., Larsen, M., et al., 2023. Diagenetic effect on reservoir quality of siliciclastic and volcaniclastic sandstones from a Paleogene volcanic rifted margin, East Greenland. J. Sediment. Res. 93 (12), 895–931. https://doi.org/10.2110/jsr.2021.127.
Worden, R.H., Burley, S.D., 2003. Sandstone diagenesis: The evolution of sand to stone. In: Burley, S.D., Worden, R.H. (Eds.), Sandstone Diagenesis: Recent and Ancient. Blackwell Pub, Oxford, pp. 1–44. https://doi.org/10.1002/9781444304459.ch.
Wu, H., Zhao, J., Wu, W., et al., 2021. Formation and diagenetic characteristics of tight sandstones in closed to semi-closed systems: Typical example from the Permian Sulige gas field. J. Petrol. Sci. Eng. 199, 108248. https://doi.org/10.1016/j.petrol.2020.108248.
Xi, K., Cao, Y., Jahren, J., et al., 2015. Diagenesis and reservoir quality of the Lower Cretaceous Quantou Formation tight sandstones in the southern Songliao Basin, China. Sediment. Geol. 330, 90–107. https://doi.org/10.1016/j.sedgeo.2015.10.007.
Xi, K., Cao, Y., Liu, K., et al., 2019. Diagenesis of tight sandstone reservoirs in the Upper Triassic Yanchang Formation, Southwestern Ordos Basin. China. Mar. Petrol. Geol. 99, 548–562. https://doi.org/10.1016/j.marpetgeo.2018.10.031.
Xu, J.H., Zhang, S.Q., Ji, Y.L., 2001. Diagenetic evolution of clastic reservoirs in the Upper and Middle Jurassic in Qiangtang Basin of northern Xizang area. J. Univ. Petroleum, China 25 (1), 4–8. https://doi.org/10.3321/j.issn:1000-5870.2001.01.002 (in Chinese).
Yang, K., Li, H., Zhou, X., et al., 2018. Diageneses and evolution of porosity of Chang 2 reservoir in Zhidan area, Ordos Basin. Geol. Sci. Technol. Inf. 37 (6), 74–81. https://doi.org/10.19509/j.cnki.dzkq.2018.0609 (in Chinese).
Yu, Y., Lin, L., Zhai, C., et al., 2019. Impacts of lithologic characteristics and diagenesis on reservoir quality of the 4th member of the Upper Triassic Xujiahe Formation tight gas sandstones in the Western Sichuan Basin, southwest China. Mar. Petrol. Geol. 107, 1–19. https://doi.org/10.1016/j.marpetgeo.2019.04.040.

Zhang, J., Xu, X., Bai, J., et al., 2022. Accumulation and exploration of continental shale gas resources of Cretaceous Shahezi Formation in Lishu Fault Depression, Songliao Basin, NE China. Petrol. Explor. Dev. 49 (3), 502–515. https://doi.org/10.1016/S1876-3804(22)60042-9.

Zhang, Y., Ma, B., Jiang, S., et al., 2024. Formation mechanisms of anomalously high reservoir quality in deep-buried volcaniclastic sandstones, central Junggar Basin, northwestern China. Mar. Petrol. Geol. 163, 106772. https://doi.org/10.1016/j.marpetgeo.2024.106772.

Zhang, Y., Xu, X., Lebedev, M., et al., 2016. Multi-scale X-ray computed tomography analysis of coal microstructure and permeability changes as a function of effective stress. Int. J. Coal Geol. 165, 149–156. https://doi.org/10.1016/j.coal.2016.08.016.

Zhao, W.B., Hu, S.Y., Deng, X.Q., et al., 2021. Physical property and hydrocarbon enrichment characteristics of tight oil reservoir in Chang 7 division of Yanchang Formation, Xin'anbian oilfield, Ordos Basin, China. Petrol. Sci. 18 (5), 1294–1304. https://doi.org/10.1016/j.petsci.2020.07.001.

Zhao, X., Yao, G., Chen, X., et al., 2022. Diagenetic facies classification and characterization of a high-temperature and high-pressure tight gas sandstone reservoir: A case study in the Ledong area, Yinggehai Basin. Mar. Petrol. Geol. 140, 105665. https://doi.org/10.1016/j.marpetgeo.2022.105665.

Zhu, N., Cao, Y., Xi, K., et al., 2019. Diagenesis and physical properties evolution of sandy conglomerate reservoirs: A case study of Triassic Baikouquan Formation in northern slope zone of Mahu Depression. J. China Univ. Min. Technol. 48 (5), 1102–1118 (in Chinese).

Zhu, S., Zhu, X., Jia, Y., et al., 2020. Diagenetic alteration, pore–throat network, and reservoir quality of tight gas sandstone reservoirs: A case study of the Upper Paleozoic sequence in the northern Tianhuan Depression in the Ordos Basin, China. AAPG Bull. 104 (11), 2297–2324. https://doi.org/10.1306/08151919058.

Zou, C.N., Tao, S.Z., Zhou, H., et al., 2008. Genesis, classification, and evaluation method of diagenetic facies. Petrol. Explor. Dev. 35 (5), 526–540. https://doi.org/10.1016/S1876-3804(09)60086-0.